

On the Use of Cramér-Rao Lower Bound for Least-Variance Circuit Parameters Identification of Li-ion Cells

Vladimir Sovljanski^{a,*}, Mario Paolone^a
vladimir.sovljanski@epfl.ch, mario.paolone@epfl.ch

^a Distributed Electrical Systems Laboratory, EPFL, 1015 Lausanne, Switzerland

*Corresponding author
EPFL STI IEM DESL
Bâtiment ELL
Station 11
CH-1015 Lausanne

June 18, 2024

Abstract

Electrochemical Impedance Spectroscopy (EIS) and Equivalent Circuit Models (ECMs) are widely used to characterize the impedance and estimate parameters of electrochemical systems such as batteries.

We use a generic ECM with ten parameters grouped to model different frequency regions of the Li-ion cell's impedance spectrum. We derive a noise covariance matrix from the measurement model and use it to assign weights for the fitting technique. The paper presents two formulations of the parameters identification problem. Using the properties of the ECM EIS spectra, we propose a method to initialize ECM parameters for the Complex Non-linear Least Squares (CNLS) technique.

The paper proposes a novel algorithm for designing the EIS experiments by applying the theory on Cramér-Rao Lower Bound (CRLB) and Fisher Information Matrix (FIM) to the identification problem. We show that contributions to the FIM elements strongly depend on the frequencies at which EIS is performed. Hence, the algorithm aims to adjust frequencies such that the most information about parameters is collected. This is done by minimizing the highest variance of ECM parameters defined by CRLB. Results of a numerical experiment show that the estimator is efficient, and frequency adjustment leads to more accurate ECM parameters' identification.

Nomenclature

ECM	Equivalent Circuit Model
EIS	Electrochemical Impedance Spectroscopy
E_0	Cell's operating voltage
ΔE	Small perturbation of cell's operating voltage
I_0	Cell's operating current
ΔI	Small perturbation of cell's operating current
j	Imaginary unit
T	Cell's temperature
SoC	Cell's State-of-Charge
$\theta, \theta_0, \hat{\theta}$	Vector of ECM parameters, their initial values and estimates
M	Number of ECM parameters
ω	Vector of all angular frequencies for EIS
N	Number of EIS measurements
$\tilde{Z}(\omega)$	Vector of cell's measured impedances
$Z(\omega, \theta)$	Vector of cell's impedance model functions
$\Re(\cdot), \Im(\cdot)$	Real and imaginary part of a complex number or function
\tilde{R}_i, \tilde{X}_i	Real and imaginary parts of cell's impedance i -th measurement
R_i, X_i	Real and imaginary parts of cell's impedance model at i -th frequency
$\arg(\cdot)$	Argument of a complex number or function
$\tilde{\rho}_i, \tilde{\varphi}_i$	Magnitude and phase of cell's impedance i -th measurement
ρ_i, φ_i	Magnitude and phase of cell's impedance model at i -th frequency
$\varepsilon_\rho, \varepsilon_\varphi$	Maximum relative error in magnitude and absolute error in phase
$\sigma_\rho, \sigma_\varphi$	Standard deviations of magnitude and phase
$\mathcal{N}(\mu, \sigma^2)$	Normal distribution with mean μ and variance σ^2
\tilde{Q}, Q	Measurement and model covariance matrix
$\tilde{\alpha}_i, \tilde{\beta}_i, \tilde{\gamma}_i$	Elements of the i -th 2×2 block of measurement covariance matrix
$\alpha_i, \beta_i, \gamma_i$	Elements of the i -th 2×2 block of model covariance matrix
\mathcal{A}	Estimated accuracy matrix
\bar{Z}_{eq}	Cell's equivalent circuit impedance
\bar{Z}_x	Complex impedance of certain part or element of cell's ECM
R_s	Series resistance
CPE	Constant Phase Element
Q_x, ϕ_x	Coefficient and exponent of CPE _{x}

Zarc	Element of ECM formed by parallel connection of CPE and a resistor
Q_W	Warburg impedance coefficient
\mathcal{L}	Locus of cell's ECM element in Nyquist plot
δ_x	Angle between the horizontal axis and CPE_x locus
r	Circle radius
k_x, n_x	Slope and intercept of a line x
$\mathbf{proj}_{\mathcal{L}}$	Normal projection of complex point to a line \mathcal{L}
D	Distance between cell's impedance measurement and its corresponding normal projection to fitted spectrum
R_{Σ}	Sum of cell's ECM resistances
ω_c	Characteristic frequency of a Zarc element of cell's ECM
τ	Time constant of a Zarc element of the cell's ECM
CRLB	Cramér-Rao Lower Bound
$p.d.f$	Probability density function
$\det(\cdot)$	Determinant of a square matrix
L	Log-likelihood function
$\mathbb{E}(\cdot)$	Expected value
ε	Vector of mismatches between the measurements and the model
CNLS	Complex Non-linear Least Squares
\mathcal{F}	Fisher Information Matrix (FIM)
$\Delta\mathcal{F}$	Contribution to the FIM element
\mathcal{C}	Inverse of the FIM
Λ	Vector of eigenvalues of the FIM
κ	Frequencies perturbation coefficient
λ	Eigenvalue of the FIM
f_{min}, f_{max}	Minimum and maximum frequency of the EIS measurements
Ω, Ω_c	Set of all indices and fixed indices of frequency points
d_i^k	Sensitivity of the minimum eigenvalue of the FIM to the perturbation of i -th frequency point at iteration k of the algorithm for frequencies adjustments
s	Sign of the highest sensitivity (by the absolute values)
V_M	Volume of the M -dimensional ellipsoid volume

1 Introduction

Estimating the Li-ion cell parameters is fundamental for designing the battery modules and packs, operating the battery and assessing its performance and degradation while serving its first or second life. The modeller may choose a specific parametric model depending on the application and desired level of detail and accuracy, which is opposed to computational complexity. Therefore, the selected model usually represents a trade-off between complexity, accuracy and computational efficiency.

In the literature, battery parametric models are classified as electrochemical and equivalent circuit models (ECMs) [1]. Considering the constraints in computational power, efficiency, and data storage, the ECM remains the predominant choice among the available battery models employed in battery management systems (BMS). Together with Electrochemical Impedance Spectroscopy (EIS), ECMs can be used to characterize the parameters of the cells in the laboratory under controlled experimental conditions. In addition, the idea of implementing on-board EIS measurements within the BMS becomes more attractive thanks to its potential to estimate the battery impedance and its ECM parameters without dismantling the battery pack [2] and to access the cells externally.

The cell and its parameters can be characterized in the time and frequency domains. In the time domain, the excitation signal is generic and can be given by the operation of the battery itself. This can lead to parameter identifiability issues if the excitation signal has only a few frequency components [3]. In [4], authors used ECM with equivalent series resistance and one branch consisting of a resistor and constant-phase element (CPE) to model the cell and estimated parameters from time-domain data. In the frequency domain, the cell is usually excited with a small sinusoidal signal (e.g., current excitation) of a defined frequency while measuring the response (e.g., cell voltage) and remaining in a pseudo-linear regime around a specific operating point. This enables characterizing the cell impedance at different frequencies. An ECM is usually assigned to EIS spectra where the choice of ECM topology and elements depends on the EIS spectra shape and is decided by the modeller before the parameters identification. A critical review [5] presents typical ECMs used in the literature for different types of cell chemistry. The authors also summarize how different parts of EIS spectra are modelled with ECM components.

The most common technique in the literature to estimate the ECM parameters from EIS data in the frequency domain is the Complex Non-linear Least Squares (CNLS) method, initially used in [6] and applied to impedance data. The CNLS aims to minimize the weighted sum of squared mismatches between the measured and chosen (theoretical) model's impedance. The theory about CNLS, applied in this paper, can be found in a dedicated chapter of [7]. Due to the highly non-convex functions expressing the ECM's equivalent impedance, and consequently the non-convex objective function of CNLS, it is always necessary to initialize parameters before solving the optimization problem using different numerical techniques, for instance, Levenberg-Marquardt algorithm [7], [8].

The literature often uses the Fisher Information Matrix (FIM) and the Cramér-Rao lower bound (CRLB) for the experiment design. CRLB defines the minimum variance for an unbiased estimator. In [9], different optimal design strategies based on FIM are classified as A-, D- and E-optimal design [10], which refers to maximizing the trace, determinant and minimum eigenvalue of FIM, respectively. Considering the optimal design of experiments on batteries, in [11], authors propose a method to maximize electrochemical single-particle model parameters identifiability by minimizing the trace of the inverse of FIM. In [12], authors use FIM to estimate the identifiability of electrochemical model parameters depending on measurements and improve the design of the experiments. Authors of [13] proposed a method based on CRLB to optimize the current profiles used to estimate ECM parameters from online measurements. In [14], they maximize the determinant of FIM by adjusting the excitation current parameters and estimating the ECM parameters containing series resistance, one R||C branch and an open-circuit voltage source in the time domain. Authors of [15] utilize FIM and CRLB to quantify the information carried by the measurements and ensure reliable ECM parameter identification. In this paper, we use the FIM to quantify the contributions that EIS measurements carry to the parameters of the ECM circuit that consists of the serial connection of pure resistor, constant phase element (CPE), two R||CPE¹ branches (Zarc) and Warburg impedance, modelling the high-, mid- and low-frequency parts of the EIS spectrum.

¹Symbol || denotes parallel electrical connection.

Different weighting options are presented in [16] as an alternative to the ideal case when the inverse of measured impedance variances is used. The alternative weighting strategies were usually applied when the measurement noise model was unknown or difficult to obtain. Nowadays, however, manufacturers of EIS measurement devices provide a detailed noise model. Still, in recent literature, authors use unity weights [17], [18]. In [19], authors assign weights equal to the inverse of the squared impedance modules. Often, covariances between real and imaginary parts in CNLS formulated in Cartesian coordinates are neglected [7]. This paper weights mismatches using an inverse of an entirely derived covariance matrix corresponding to the measurement noise model.

Initialization of the parameters for CNLS is often done by defining the physically meaningful ranges of parameters' values according to experience and choosing the values within the corresponding ranges. Authors of [20] initialize parameters for the Randles circuit by looking at some properties of the EIS spectra to extract the parameters' values quickly. However, for some parameters, the feasible range can be challenging to guess. In [19], a method is proposed for re-adjusting the feasible range for battery model parameters to automatize the fitting process. Still, the initial range for each parameter requires a manual adjustment. In [21], authors manually divide EIS spectra into regions corresponding to different parts of ECM and separately solve least-squares to obtain estimates. This approach might provide results for initialization rather than final estimates since, here, it is assumed that there is no overlapping between different elements in the spectra.

To the best of our knowledge, EIS measurements are usually performed at logarithmically distributed frequencies within the pre-defined frequency range and number of points per decade (ppd). When estimating the parameters, the variances of estimates are rarely compared to the theoretical minimum defined by CRLB. Therefore, this paper proposes the experimental design for characterizing the Li-ion battery impedance and accurately estimating ECM parameters from EIS measurements.

In view of the above state-of-the-art on ECM parameters identification from EIS data, the authors of this study identified two fundamental research questions:

- i. How to set frequencies that bring the most information in the parameters identification process?
- ii. How to best initialize the ECM parameters for solving the CNLS?

The key contributions of this work are summarized as follows:

- (1) We first formulate the identification problem for Li-ion ECM parameters estimation from EIS measurements in a rigorous mathematical way in both polar and Cartesian coordinates. We derive a covariance matrix from the measurement model commonly provided by EIS instrument manufacturers. Its inverse weights the mismatch vectors between the measurements and model functions. We discuss the theory and analyze the connection between the obtained EIS spectra and elements of wide-band Li-ion ECM with ten parameters. This results in the development of a method for the automated initialization of the parameters that leverages the properties of the EIS spectra and parameters importance in different frequency regions.
- (2) We estimate the Li-ion cell ECM parameters using the weighted CNLS by solving the unconstrained minimization problem starting from the obtained initial parameter values. This provides the estimation algorithm to converge to the values with expected statistics, i.e., mean value and variance of the estimated parameters.
- (3) We derive the expressions for computing the FIM and CRLB for estimated parameters of Li-ion ECM from the EIS data in a general Gaussian form. This is used to quantify the best possible accuracy and to show that our estimator is efficient.
- (4) We improve the experimental design by proposing a novel algorithm to adjust the frequencies at which EIS should be performed to increase the accuracy of the estimates using the E-optimal design. We show that information about ECM parameters strongly depends on the frequencies at which EIS measurements are performed. The algorithm decides the frequency distribution over a predefined range by maximizing the FIM's lowest eigenvalue and minimizing the highest eigenvalue of its inverse matrix. EIS measurements at these frequencies contain more information about ECM parameters than traditionally used logarithmic span.

Therefore, the final frequency adjustment leads to the EIS measurements from which ECM parameters can be estimated with lower variances and higher overall fitting accuracy.

This paper is organized as follows: in Section 2, we present the Li-ion battery ECM parameters estimation problem from EIS measurements in a rigorous way and discuss two different formulations and the problem of parameters' initialization, recall the theory of general Gaussian CRLB adapted to our problem and introduce a novel algorithm for improving the variance of the estimated parameters via CRLB. Section 3 presents the results of the numerical simulations and experimental validation on a real Li-ion cell, where the parameters are estimated, and the overall estimation accuracy improved thanks to the proposed algorithm. Section 4 summarizes the main contributions and potentials of this work.

Keywords

Li-ion batteries, Electrochemical Impedance Spectroscopy, Equivalent Circuit Models, parameters estimation, Cramér-Rao Lower Bound, Fisher Information Matrix.

2 Method

2.1 General Aspects and Assumptions of Cells' Parameters Identification via EIS Measurements

EIS is a powerful, non-invasive technique used to characterize Lithium-ion cells and generic electrochemical energy storage devices. EIS is performed by exciting the battery cell with small sinusoidal signals (current in galvanostatic mode or voltage in potentiostatic mode) at different frequencies and measuring the cell's response (respectively, the voltage in galvanostatic mode or current in potentiostatic mode). Although electrochemical systems are nonlinear, for sufficiently small excitations (yet maintaining an acceptable signal-to-noise ratio), their response can be approximated as being pseudo-linear [22]. Small excitation amplitudes ensure that, while performing the EIS, changes in the State-of-Charge (SoC) and cell temperature are negligible, i.e., $\Delta\text{SoC} \approx 0$ and $\Delta T \approx 0$. Supposing that the voltage and current signals are $E(t) = E_0 + \Delta E \sin(\omega t)$ and $I(t) = I_0 + \Delta I \sin(\omega t - \varphi)$, respectively, while operating around the point (E_0, I_0) on the nonlinear voltage-current curve, the complex impedance can be simply calculated as:

$$\bar{Z}(\omega) = \frac{\Delta \bar{E}(\omega)}{\Delta \bar{I}(\omega)} = R(\omega) + jX(\omega), \quad (1)$$

where $\Delta \bar{E}(\omega) = \Delta E(\omega) \angle 0$ and $\Delta \bar{I}(\omega) = \Delta I(\omega) \angle (-\varphi)$ are corresponding phasors of sinusoidal perturbation signals $\Delta E \sin(\omega t)$ and $\Delta I \sin(\omega t - \varphi)$.

The common method used to estimate the ECM parameters is the Complex Non-linear Least Square (CNLS). This is done by simultaneously fitting the real and imaginary parts of complex impedance measurements to fixed model functions, which are usually non-linear. Various terms in the CNLS objective are weighted to quantify the heteroscedastic noise content of each observation.

The choice of elements comprising the ECM depends on the shape of the obtained complex impedance curve on the Nyquist plot and it is fixed by the modeller before the fitting procedure. Once the ECM topology is fixed, the equivalent impedance $\tilde{Z}(\boldsymbol{\theta}, \omega)$ is expressed as a function of the parameter vector, $\boldsymbol{\theta}$, and angular frequency ω .

In this paper, the assumptions are the following: (a) the small sine excitation signal is always chosen such that the system's response is pseudo-linear, (b) the measurement noise model is known, (c) we use a given parametric circuit model of a Li-ion battery cell.

The ECM parameters $\boldsymbol{\theta}$ are estimated by solving the following unconstrained optimization problem either in Cartesian or polar coordinates, written in the standard quadratic form:

$$\hat{\boldsymbol{\theta}} = \underset{\boldsymbol{\theta}}{\operatorname{argmin}} \left(\tilde{\mathcal{Z}}(\boldsymbol{\omega}) - \mathcal{Z}(\boldsymbol{\theta}, \boldsymbol{\omega}) \right)^\top \tilde{\mathbf{Q}}^{-1} \left(\tilde{\mathcal{Z}}(\boldsymbol{\omega}) - \mathcal{Z}(\boldsymbol{\theta}, \boldsymbol{\omega}) \right), \quad (2)$$

where vector $\tilde{\mathcal{Z}}(\boldsymbol{\omega}) = [\tilde{z}_1, \dots, \tilde{z}_N]^\top$, with $\tilde{z}_i = [\tilde{R}_i, \tilde{X}_i]^\top$, $\tilde{R}_i = \Re(\tilde{Z}(\omega_i))$ and $\tilde{X}_i = \Im(\tilde{Z}(\omega_i))$ in Cartesian or $\tilde{z}_i = [\tilde{\rho}_i, \tilde{\varphi}_i]^\top$, $\tilde{\rho}_i = |\tilde{Z}(\omega_i)|$ and $\tilde{\varphi}_i = \arg(\tilde{Z}(\omega_i))$ in polar coordinates, contains separated real and imaginary parts in Cartesian, or modules and angles in polar coordinates, of impedances measured at N frequencies contained in the vector $\boldsymbol{\omega} = [\omega_1, \dots, \omega_N]^\top$. On the other hand, $\mathcal{Z}(\boldsymbol{\theta}, \boldsymbol{\omega})$ contains the impedance model (expressions for the real and imaginary part, or module and angle, of ECM impedance) as a function of ECM parameters $\boldsymbol{\theta}$ and evaluated at corresponding frequencies. The mismatches between the measurements and model are weighted using the inverse of the measurement covariance matrix, $\tilde{\mathbf{Q}}$.

Regardless of the formulation, the measurement covariance matrix $\tilde{\mathbf{Q}}$ has a block-diagonal form, $\tilde{\mathbf{Q}} = \operatorname{diag}(\tilde{\mathbf{Q}}_1, \dots, \tilde{\mathbf{Q}}_N)$ since the measurements are independent. Therefore, the problem (2) can be also written as:

$$\hat{\boldsymbol{\theta}} = \underset{\boldsymbol{\theta}}{\operatorname{argmin}} \sum_{i=1}^N (\tilde{z}_i - z_i(\boldsymbol{\theta}))^\top \tilde{\mathbf{Q}}_i^{-1} (\tilde{z}_i - z_i(\boldsymbol{\theta})). \quad (3)$$

The objective function given by Eq. (3) is generally highly non-convex due to the non-convexity of model functions $z_i(\boldsymbol{\theta})$. Hence, it can have multiple local minima, which motivates the need for good initialization of parameters that will be elaborated on later on in the paper.

2.2 Measurement Model

In system identification, the choice of the noise model is essential for selecting the estimation method to be used [23]. In what follows, we provide the measurement model structure that is used in the proposed ECM parameters estimation technique.

The EIS instrument's precision is often characterized by maximum relative error in magnitude, ε_ρ , and maximum absolute error in phase, ε_φ . Manufacturers often provide accuracy contour plots where one can read the values of ε_ρ and ε_φ as a function of the impedance magnitude and frequency. The accuracy contours divide the frequency-impedance plane into several areas. Each accuracy contour plot area is defined as a set of $(f, |\bar{Z}|)$ points with $f > 0$ and $|\bar{Z}| > 0$, at which the EIS instrument measures the impedance magnitude $|\bar{Z}|$ with maximum magnitude relative error ε_ρ and absolute error ε_φ , at frequency f . Typical contour plots and instructions for interpreting them can be found, for instance, in [24] and [25] with respect to commercial EIS instruments.

To express the standard deviations of the measured impedance module and phase, we use the three-sigma (3σ) rule, assuming that the measurement noise is Gaussian, unbiased, and lies within the specified maximum bound with a probability of 99.73%. Therefore, to obtain the standard deviations in magnitude and phase, we divide the maximum error provided by the manufacturer of the EIS instrument by 3. This yields:

$$\sigma_\rho(\rho) = \frac{1}{3}\rho \cdot \varepsilon_\rho \quad \text{and} \quad \sigma_\varphi = \frac{1}{3} \cdot \varepsilon_\varphi = \text{const.} \quad (4)$$

Hence, for a true value of complex impedance $\bar{Z} = \rho e^{j\varphi}$, corresponding measured impedance is $\tilde{Z} = \tilde{\rho} e^{j\tilde{\varphi}} = (\rho + \Delta\rho)e^{j(\varphi + \Delta\varphi)}$ where the magnitude and phase errors are distributed as $\Delta\rho \sim \mathcal{N}(0, \frac{\rho\varepsilon_\rho}{3})$ and $\Delta\varphi \sim \mathcal{N}(0, \frac{\varepsilon_\varphi}{3})$, respectively.

2.3 ECM Parameters Estimation via the CNLS in Polar Coordinates

In polar coordinates, (3) can be written as:

$$\hat{\boldsymbol{\theta}} = \underset{\boldsymbol{\theta}}{\operatorname{argmin}} \sum_{i=1}^N \left(\begin{bmatrix} \tilde{\rho}_i \\ \tilde{\varphi}_i \end{bmatrix} - \begin{bmatrix} \rho_i(\boldsymbol{\theta}) \\ \varphi_i(\boldsymbol{\theta}) \end{bmatrix} \right)^\top \begin{bmatrix} \sigma_\rho^2(\rho_i) & 0 \\ 0 & \sigma_\varphi^2 \end{bmatrix}^{-1} \left(\begin{bmatrix} \tilde{\rho}_i \\ \tilde{\varphi}_i \end{bmatrix} - \begin{bmatrix} \rho_i(\boldsymbol{\theta}) \\ \varphi_i(\boldsymbol{\theta}) \end{bmatrix} \right). \quad (5)$$

In this case, the covariance matrix has a pure diagonal form:

$$\tilde{\mathbf{Q}} = \mathbf{diag}(\sigma_{\rho_1}^2, \sigma_{\varphi}^2, \dots, \sigma_{\rho_N}^2, \sigma_{\varphi}^2) \quad (6)$$

since it is assumed that stochastic errors in magnitude and phase are not correlated and, in addition, stochastic errors at different frequencies are not correlated with each other. The relationship between the measured impedance module and angle and real and imaginary parts is:

$$|\bar{Z}(\omega_i)| = \rho_i = \sqrt{R_i^2 + X_i^2} \quad (7)$$

$$\arg \bar{Z}(\omega_i) = \varphi_i = \arctan \left(\frac{X_i}{R_i} \right), \quad \text{since } R_i > 0. \quad (8)$$

Same relations hold for model functions in polar coordinates $\rho_i(\boldsymbol{\theta})$ and $\varphi_i(\boldsymbol{\theta})$ expressed in terms of model functions in Cartesian coordinates, $R_i(\boldsymbol{\theta})$ and $X_i(\boldsymbol{\theta})$.

2.4 ECM Parameters Estimation via the CNLS in Cartesian Coordinates

In Cartesian coordinates, the minimization problem (3) becomes:

$$\hat{\boldsymbol{\theta}} = \underset{\boldsymbol{\theta}}{\operatorname{argmin}} \sum_{i=1}^N \left(\begin{bmatrix} \tilde{R}_i \\ \tilde{X}_i \end{bmatrix} - \begin{bmatrix} R_i(\boldsymbol{\theta}) \\ X_i(\boldsymbol{\theta}) \end{bmatrix} \right)^\top \tilde{\mathbf{Q}}_i^{-1} \left(\begin{bmatrix} \tilde{R}_i \\ \tilde{X}_i \end{bmatrix} - \begin{bmatrix} R_i(\boldsymbol{\theta}) \\ X_i(\boldsymbol{\theta}) \end{bmatrix} \right). \quad (9)$$

Since the measurement errors are given in polar coordinates, while the measurements and model functions in Cartesian, we perform a transformation of coordinates (i.e., projection from polar to Cartesian coordinates), as in [26] and [27], to obtain $\tilde{\mathbf{Q}}_i$. Namely:

$$\tilde{\mathbf{Q}}_i = \begin{bmatrix} \sigma^2(\tilde{R}_i) & \sigma(\tilde{R}_i, \tilde{X}_i) \\ \sigma(\tilde{R}_i, \tilde{X}_i) & \sigma^2(\tilde{X}_i) \end{bmatrix} = \begin{bmatrix} \tilde{\alpha}_i & \tilde{\beta}_i \\ \tilde{\beta}_i & \tilde{\gamma}_i \end{bmatrix}, \quad (10)$$

whose elements are calculated using the measured impedance quantities (magnitude $\tilde{\rho}$ and phase $\tilde{\varphi}$):

$$\tilde{\alpha}_i = \tilde{\rho}_i^2 e^{-2\sigma_\varphi^2} [\cos^2 \tilde{\varphi}_i (\cosh(2\sigma_\varphi^2) - \cosh(\sigma_\varphi^2)) + \sin^2 \tilde{\varphi}_i (\sinh(2\sigma_\varphi^2) - \sinh(\sigma_\varphi^2))] \quad (11)$$

$$+ \sigma_{\rho_i}^2 e^{-2\sigma_\varphi^2} [\cos^2 \tilde{\varphi}_i (2 \cosh(2\sigma_\varphi^2) - \cosh(\sigma_\varphi^2)) + \sin^2 \tilde{\varphi}_i (2 \sinh(2\sigma_\varphi^2) - \sinh(\sigma_\varphi^2))] \quad (12)$$

$$\tilde{\beta}_i = \tilde{\rho}_i^2 e^{-\sigma_\varphi^2} [\sin^2 \tilde{\varphi}_i (\cosh(2\sigma_\varphi^2) - \cosh(\sigma_\varphi^2)) + \cos^2 \tilde{\varphi}_i (\sinh(2\sigma_\varphi^2) - \sinh(\sigma_\varphi^2))] \quad (13)$$

$$+ \sigma_{\rho_i}^2 e^{-\sigma_\varphi^2} [\sin^2 \tilde{\varphi}_i (2 \cosh(2\sigma_\varphi^2) - \cosh(\sigma_\varphi^2)) + \cos^2 \tilde{\varphi}_i (2 \sinh(2\sigma_\varphi^2) - \sinh(\sigma_\varphi^2))] \quad (14)$$

$$\tilde{\gamma}_i = \sin \tilde{\varphi}_i \cos \tilde{\varphi}_i e^{-4\sigma_\varphi^2} [\sigma_{\rho_i}^2 + (\sigma_{\rho_i}^2 + \tilde{\rho}_i^2)(1 - e^{\sigma_\varphi^2})]. \quad (15)$$

2.5 Accuracy Assessment of the Estimates

Variances for the estimated parameters can be approximately calculated as diagonal elements of the matrix \mathbf{A}^{-1} , calculated at values of estimated parameters, $\hat{\boldsymbol{\theta}}$ where, the element (k, l) is expressed as:

$$\mathbf{A}_{k,l} \approx \left\{ \left[\frac{\partial \mathbf{Z}(\boldsymbol{\theta}, \boldsymbol{\omega})}{\partial \theta_k} \right]^\top \tilde{\mathbf{Q}}^{-1} \left[\frac{\partial \mathbf{Z}(\boldsymbol{\theta}, \boldsymbol{\omega})}{\partial \theta_l} \right] - \left[\tilde{\mathbf{Z}}(\boldsymbol{\omega}) - \mathbf{Z}(\boldsymbol{\theta}, \boldsymbol{\omega}) \right]^\top \tilde{\mathbf{Q}}^{-1} \left[\frac{\partial^2 \mathbf{Z}(\boldsymbol{\theta}, \boldsymbol{\omega})}{\partial \theta_k \partial \theta_l} \right] \right\} \Bigg|_{\boldsymbol{\theta}=\hat{\boldsymbol{\theta}}} \quad (14)$$

which corresponds to one-half of the corresponding (k, l) -th Hessian matrix element [7].

2.6 ECM Parameters Initial Guess

Since the objective function of the minimization problem given by Eq. (3) is highly non-convex, the solution is very sensitive to the initial guess of the ECM parameters. Further, if the initial point is far from the true value, the solver is more likely to find a local minimum. Therefore, there is a need to improve the initial guess of parameters $\boldsymbol{\theta}$ and make the optimization solver more likely to find the estimates with the expectation equal to the actual true values. One possible approach can be to analyze the geometrical shapes of certain parts of EIS spectra.

As a matter of fact, when connected, the spectra of each ECM element interfere and, therefore, their corresponding spectra overlap. Still, approximate values for ECM parameters can be extracted by fitting parts of the spectra to the expected geometrical shapes of each ECM branch.

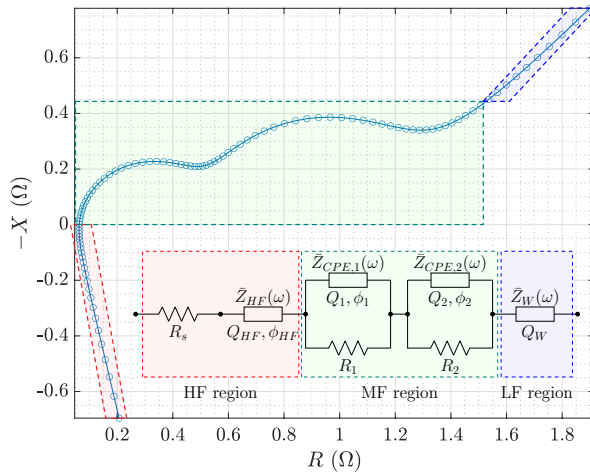


Figure 1: Impedance spectrum of the Li-ion cell ECM. The parameters are indicated below each element.

Param.	Values θ	Unit
R_s	3.80E-02	Ω
Q_{HF}	1.67E+04	$S \cdot s^{-\varphi_{HF}}$
ϕ_{HF}	-8.50E-01	-
R_1	4.50E-01	Ω
Q_1	2.00E-02	$S \cdot s^{-\varphi_1}$
ϕ_1	9.00E-01	-
R_2	6.50E-01	Ω
Q_2	4.00E-01	$S \cdot s^{-\varphi_2}$
ϕ_2	9.00E-01	-
Q_W	3.69E+00	$S \cdot s^{-1/2}$

Table 1: ECM parameters' true values (inspired from [18]).

Fig. 1 shows the noiseless impedance spectrum and ECM used to model the Li-ion battery cell in this paper and highlights different frequency regions. Tab. 1 reports the ECM parameters' true values. As known, the equivalent cell's impedance can be represented as a superposition of equivalent series resistance, CPE modelling the HF behaviour, a number (e.g., two) of Zarc elements (i.e., CPE in parallel to a resistor) and the Warburg impedance:

$$\bar{Z}_{eq}(\boldsymbol{\theta}; \omega) = R_s + \bar{Z}_{HF} + R_1 \parallel \bar{Z}_{CPE,1} + R_2 \parallel \bar{Z}_{CPE,2} + \bar{Z}_W, \quad (15)$$

where $\bar{Z}_1 \parallel \bar{Z}_2 = \frac{\bar{Z}_1 \bar{Z}_2}{\bar{Z}_1 + \bar{Z}_2}$ is the equivalent impedance of parallel connection of \bar{Z}_1 and \bar{Z}_2 . The expression for HF region CPE is

$$\bar{Z}_{HF}(Q_{HF}, \phi_{HF}; \omega) = \frac{1}{(j\omega)^{\phi_{HF}} Q_{HF}}, \quad \phi_{HF} \in [-1, 0), \quad (16)$$

while for two CPEs within the MF region, we have:

$$\bar{Z}_{CPE,i}(Q_i, \phi_i; \omega) = \frac{1}{(j\omega)^{\phi_i} Q_i}, \quad \phi_i \in (0, 1], \quad i \in \{1, 2\}. \quad (17)$$

The Warburg impedance is a special case of CPE with the exponent ϕ equal to $\frac{1}{2}$:

$$\bar{Z}_W(Q_W; \omega) = \frac{1}{\sqrt{j\omega} \cdot Q_W}. \quad (18)$$

Separating the real $\Re(\bar{Z}_{eq}(\boldsymbol{\theta}; \omega)) = R_{eq}(\boldsymbol{\theta}, \omega)$ and imaginary $\Im(\bar{Z}_{eq}(\boldsymbol{\theta}; \omega)) = X_{eq}(\boldsymbol{\theta}, \omega)$ parts of the equivalent impedance yields:

$$R_{eq}(\boldsymbol{\theta}, \omega) = R_s + \frac{1}{\omega^{\phi_{HF}} Q_{HF}} \cos \delta_{HF} + \sum_{i=1}^2 \frac{R_i + R_i^2 Q_i \omega^{\phi_i} \cos \delta_i}{1 + 2R_i Q_i \omega^{\phi_i} \cos \delta_i + (R_i Q_i \omega^{\phi_i})^2} + \frac{1}{Q_W \sqrt{2\omega}} \quad (19)$$

$$X_{eq}(\boldsymbol{\theta}, \omega) = -\frac{1}{\omega^{\phi_{HF}} Q_{HF}} \sin \delta_{HF} - \sum_{i=1}^2 \frac{R_i^2 Q_i \omega^{\phi_i} \cos \delta_i}{1 + 2R_i Q_i \omega^{\phi_i} \cos \delta_i + (R_i Q_i \omega^{\phi_i})^2} - \frac{1}{Q_W \sqrt{2\omega}} \quad (20)$$

where $\delta_{HF} = \frac{\phi_{HF}\pi}{2}$ and $\delta_i = \frac{\phi_i\pi}{2}$, $i \in \{1, 2\}$.

2.6.1 On the Geometry of ECM Elements Spectra

Individually, all the ECM electrical elements, with fixed parameters, produce spectra with a known locus \mathcal{L} governed by the expressions for its impedance:

$$\mathcal{L} = \{(R(\omega), -X(\omega)) : R(\omega) = \Re(\bar{Z}(\omega)) \wedge X(\omega) = \Im(\bar{Z}(\omega)) \wedge \omega \in (0, \infty)\}. \quad (21)$$

Note that we always consider the Nyquist plot with axes indicating R and $-X$ as a usual convention for plotting the EIS measurements.

The locus of the resistance R_s is simply a singleton $(R_s, 0)$ at the Nyquist plot. Adding a pure resistance in series to the ECM translates the entire spectrum in the direction of the horizontal axis by the value of the resistance.

The locus of CPE with parameters Q and ϕ represents a line starting from the origin and an angular coefficient $\tan \frac{\pi\phi}{2}$.

By adding the resistance R in parallel to the CPE (i.e., the Zarc element), the locus represents a part of a depressed circle crossing the real axis at $(0, 0)$ and $(R, 0)$, centred at $\left(\frac{R}{2}, -\frac{R}{2} \cot \frac{\pi\phi}{2}\right)$, with a radius $r = \frac{R}{2 \sin \frac{\pi\phi}{2}}$ and $\Im\{\bar{Z}_{arc}\} < 0$.

The CPE can be seen as a special case of a Zarc element for which $R \rightarrow \infty$ and, therefore, the locus of the CPE impedance is tangent to Zarc if their exponents are equal.

Different elements dominate in different frequency regions as indicated in Fig. 1. However, the spectra produced by individual elements interfere. This results in the equivalent superposed spectrum for which the locus of different frequency regions deviates from the ideal geometrical

shapes (as was the case for individual ECM elements). Still, the approximate values for ECM parameters can be extracted and used to define each ECM parameter's initial guess and reasonable interval of feasibility. In such a way, we reduce the solution space of the estimation problem.

Theoretically, as $\omega \rightarrow 0$, the Warburg impedance modelling the LF region dominates the EIS spectrum while the influence of HF and MF parts is negligible. Since:

$$k_{LF} = \lim_{\omega \rightarrow 0} \frac{\Im(\bar{Z}_{eq}(\boldsymbol{\theta}; \omega))}{\Re(\bar{Z}_{eq}(\boldsymbol{\theta}; \omega))} = -1 \quad (22)$$

and

$$n_{LF} = \lim_{\omega \rightarrow 0} [\Im(\bar{Z}_{eq}(\boldsymbol{\theta}; \omega)) - k_{LF}\Re(\bar{Z}_{eq}(\boldsymbol{\theta}; \omega))] = R_s + R_1 + R_2 = R_\Sigma, \quad (23)$$

on the Nyquist plot ($R, -X$), the spectrum asymptotically approaches the line $-X = R + R_\Sigma$.

Similarly, as $\omega \rightarrow \infty$, the HF spectrum asymptotically approach the line $X = k_{HF}R + n_{HF}$ where:

$$k_{HF} = \lim_{\omega \rightarrow \infty} \frac{\Im(\bar{Z}_{eq}(\boldsymbol{\theta}; \omega))}{\Re(\bar{Z}_{eq}(\boldsymbol{\theta}; \omega))} = \lim_{\omega \rightarrow \infty} \frac{\Im(\bar{Z}_{eq}(\boldsymbol{\theta}; \omega))}{\Re(\bar{Z}_{eq}(\boldsymbol{\theta}; \omega)) - R_s} = -\tan\left(\frac{\pi\phi_{HF}}{2}\right) \quad (24)$$

and

$$n_{HF} = \lim_{\omega \rightarrow \infty} [\Im(\bar{Z}_{eq}(\boldsymbol{\theta}; \omega)) - k_{HF}\Re(\bar{Z}_{eq}(\boldsymbol{\theta}; \omega))] = R_s \tan\left(\frac{\pi\phi_{HF}}{2}\right). \quad (25)$$

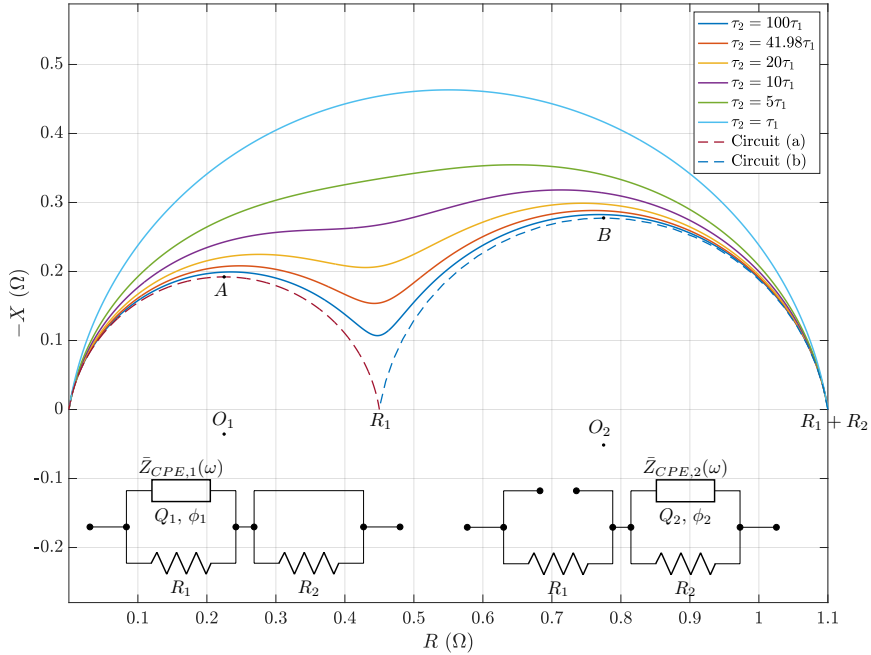


Figure 2: Equivalent MF region spectrum cleaned from the interference produced by \bar{Z}_{HF} and \bar{Z}_{LF} for different ratios of the time constants of Zarc₁ and Zarc₂ (cell's parameters R_1, Q_1, ϕ_1, R_2 and ϕ_2 true values are those reported in Tab. 1, while parameter Q_2 changes its values to achieve a desired $\frac{\tau_2}{\tau_1}$ ratio).

We assume that two Zarc elements have different time constants τ_1 and τ_2 , $\tau_1 < \tau_2$, defined by

$$\tau_1 = (R_1 Q_1)^{\frac{1}{\phi_1}} \quad \text{and} \quad \tau_2 = (R_2 Q_2)^{\frac{1}{\phi_2}}. \quad (26)$$

An example of the spectra of MF region produced only by two Zarc elements is shown in Fig. 2 for different time constants of Zarcs by varying only the parameter Q_2 . For parameters' values reported in Tab. 1, $\tau_2 = 41.98\tau_1$. The superposed MF spectrum of the two Zarcs is positioned above parts of two depressed semi-circles located above the horizontal axis, centred at O_1 and O_2

with radii $\frac{R_1}{2 \sin \frac{\pi\phi_1}{2}}$ and $\frac{R_2}{2 \sin \frac{\pi\phi_2}{2}}$, respectively. Both represent the locus of the MF region ECM with two ZarcS connected in series: in the first one, CPE₂, is short-circuited, while in the second one, CPE₁ is replaced by an open-circuit. The interference of two Zarc elements spectra depends on the ratio between time constants, $\frac{\tau_2}{\tau_1}$. The greater the ratio, the closer is the superposed spectra to these depressed semi-circles. For these two ZarcS, the characteristic angular frequencies are given by

$$\omega_{c1} = \frac{1}{(R_1 Q_1)^{\frac{1}{\phi_1}}} \quad \text{and} \quad \omega_{c2} = \frac{1}{(R_2 Q_2)^{\frac{1}{\phi_2}}}. \quad (27)$$

The MF impedance (excluding the HF and LF impedances) is

$$\bar{Z}_{MF}(\boldsymbol{\theta}; \omega) = R_1 \parallel \bar{Z}_{CPE,1} + R_2 \parallel \bar{Z}_{CPE,2} = \frac{R_1}{1 + (j\omega)^{\phi_1} R_1 Q_1} + \frac{R_2}{1 + (j\omega)^{\phi_2} R_2 Q_2} \quad (28)$$

and at ω_{c1} and ω_{c2} it has the following values:

$$\bar{Z}_{MF}(\boldsymbol{\theta}_{MF}; \omega_{c1}) = \frac{R_1}{1 + j^{\phi_1}} + \frac{R_2}{1 + j^{\phi_2} \left(\frac{\tau_2}{\tau_1}\right)^{\phi_2}} \quad (29)$$

$$\bar{Z}_{MF}(\boldsymbol{\theta}_{MF}; \omega_{c2}) = \frac{R_1}{1 + j^{\phi_1} \left(\frac{\tau_1}{\tau_2}\right)^{\phi_1}} + \frac{R_2}{1 + j^{\phi_2}}. \quad (30)$$

If $\tau_1 \ll \tau_2$ (i.e., the processes inside the cell modelled with Zarc elements can be well distinguished) we have:

$$\bar{Z}_{MF}(\boldsymbol{\theta}_{MF}; \omega_{c1}) \approx \frac{R_1}{1 + j^{\phi_1}} + R_2(0 + j0) = \frac{R_1}{2} - j \frac{R_1}{2} \tan \frac{\pi\phi_1}{4}, \quad (31)$$

$$\bar{Z}_{MF}(\boldsymbol{\theta}_{MF}; \omega_{c2}) \approx R_1(1 + j0) + \frac{R_2}{1 + j^{\phi_2}} = R_1 + \frac{R_2}{2} - j \frac{R_2}{2} \tan \frac{\pi\phi_2}{4} \quad (32)$$

which are exactly the peaks of the two depressed semi-circles defined by Zarc1 and Zarc2 elements while having the CPE2 and CPE1 replaced by a short-circuit and open-circuit, respectively. In Fig. 2, these two peaks are denoted as *A* and *B*.

2.6.2 Parameters Initialization Procedure

In what follows, we propose a detailed procedure to initialize the ECM parameters for the CNLS using the discussed properties of the spectra. First, the LF and HF parameters are estimated from two ends of the EIS spectrum.

Fitting the LF and HF spectra to a line. We first choose the number of points N_{LF} and N_{HF} used for fitting such that the residuals between the selected points of the LF and HF spectra and the fitted line are normally distributed while respecting the maximum relative error in magnitude and maximum absolute error in phase as defined in Section 2.2. This ensures that the points belong to the part of the spectrum where the Warburg impedance and CPE used to model the LF and HF spectrum dominate, respectively. The procedure is described in the following pseudo-code.

Algorithm 1 Determining N_{xF} , k_{xF} and n_{xF} , $x \in \{L, H\}$

- 1: **Initialize** $N_{xF} \leftarrow 1$, $\varepsilon_\rho = \varepsilon_\rho(f, |Z|)$, $\varepsilon_\varphi = \text{const}$;
- 2: Sort the EIS data on f in decreasing (for HF) or increasing order (for LF);
- 3: **do**
- 4: $N_{xF} \leftarrow N_{xF} + 1$;
- 5: Obtain k_{xF} and n_{xF} by solving:

$$\begin{aligned}
 & \underset{k_{xF}, n_{xF}}{\operatorname{argmin}} \quad \sum_{i=1}^{N_{xF}} D_i^2 \\
 & \text{s.t.} \quad D_i = \left| \tilde{Z}_i - Z_i^\mathcal{L} \right| \\
 & \quad \mathcal{L}(R_i) = k_{xF} R_i + n_{xF} \\
 & \quad k_{xF} \in \begin{cases} \{-1\}, & x = L \\ [0, +\infty), & x = H \end{cases} \\
 & \quad Z_i^\mathcal{L} = \mathbf{proj}_\mathcal{L} \tilde{Z}_i
 \end{aligned} \tag{33}$$

- 6: $\tilde{\varepsilon}_{\rho_i} = \left| \frac{|Z_i^\mathcal{L}| - |\tilde{Z}_i|}{|Z_i^\mathcal{L}|} \right|$, $\tilde{\varepsilon}_{\varphi_i} = \left| \arg Z_i^\mathcal{L} - \arg \tilde{Z}_i \right|$
 - 7: **while** $\tilde{\varepsilon}_{\rho_i} \leq \varepsilon_\rho(f_i, \tilde{\rho}_i)$ **and** $\tilde{\varepsilon}_{\varphi_i} \leq \varepsilon_\varphi, \forall i \in \{1, \dots, N_{xF}\}$
-

The algorithm initializes the starting number of data points N_{xF} and the measurement model through ε_ρ and ε_φ . At each iteration, it increases the number of data points used for fitting and finds the slope and the interception by fitting N_{xF} consecutive end-points of the spectra (either from the LF or HF) to a line. Namely, it solves a simple least-squares problem (33) by minimizing the sum of squared distances D_i between the measurements \tilde{Z}_i and their corresponding normal projections (in Algorithm 1, $\mathbf{proj}_\mathcal{L}$ denotes the projection operator) to a line \mathcal{L} , denoted as $Z_i^\mathcal{L}$ for $i = 1, \dots, N$. It uses the property that the HF and LF spectra asymptotically approach the line with slope $k_{HF} \in [0, +\infty)$ and $k_{LF} = -1$, respectively. The algorithm then computes all the relative errors in magnitude and absolute errors in phase between the measured points and corresponding fitted points on the line. It terminates if any of the errors exceed the defined error limits. **Initialization of LF parameter Q_W .** Starting from the lowest frequency, N_{LF} points are used to fit the spectra to a line $X(R) = k_{LF}R + n_{LF}$, specifically $-X = R + R_\Sigma$ for which:

$$\tilde{R}_i + j\tilde{X}_i \approx R_\Sigma + \bar{Z}_W = R_\Sigma + \frac{1}{Q_W \sqrt{\omega_i}} e^{-j\frac{\pi}{4}}, \quad i = 1, \dots, N_{LF}. \tag{34}$$

Therefore, Q_W can be initialized with the mean value using the expressions for Q_W from both real and imaginary parts of these selected points:

$$Q_W^0 = \frac{1}{2N_{LF}} \left(\sum_{i=1}^{N_{LF}} \frac{1}{\sqrt{2\omega_i}(\tilde{R}_i - R_\Sigma)} - \sum_{i=1}^{N_{LF}} \frac{1}{\sqrt{2\omega_i}\tilde{X}_i} \right), \tag{35}$$

where R_Σ is the interception of the fitted line with the horizontal axis. Therefore, fitting the LF part of the spectra has provided us with the initial guess for Q_W and the sum of all the resistances of the ECM, $R_\Sigma = R_s + R_1 + R_2$.

Initialization of HF parameters R_s , Q_{HF} and ϕ_{HF} . Choosing the N_{HF} points with the highest frequencies, for which again the residuals are normally distributed, we fit the HF spectra to a line $-X = k_{HF}R + n_{HF}$ where the chosen points are expressed as:

$$\tilde{R}_i + j\tilde{X}_i \approx R_s + \bar{Z}_{HF} = R_s + \frac{1}{\omega_i^{\phi_{HF}} Q_{HF}} e^{-j\frac{\pi\phi_{HF}}{2}}, \quad i = 1, \dots, N_{HF}. \tag{36}$$

On obtaining the slope k_{HF} , the exponent ϕ_{HF} is initialized with

$$\phi_{HF}^0 \approx \frac{\arctan k_{HF}}{\pi/2}. \tag{37}$$

Now, the initial guess for R_s can be obtained by simply using (25) as

$$R_s^0 \approx \frac{n_{HF}}{\tan\left(\frac{\pi\phi_{HF}^0}{2}\right)}, \quad (38)$$

and Q_{HF} can be initialized by averaging the expressions for Q_{HF} from the real and imaginary part of (36) evaluated at \tilde{R}_i and \tilde{X}_i over the chosen N_{HF} points:

$$Q_{HF}^0 = \frac{1}{2N_{HF}} \left(\sum_{i=1}^{N_{HF}} \frac{1}{(\tilde{R}_i - R_s^0)\omega_i^{\phi_{HF}^0}} \cos \frac{\pi\phi_{HF}^0}{2} - \sum_{i=1}^{N_{HF}} \frac{1}{\tilde{X}_i\omega_i^{\phi_{HF}^0}} \sin \frac{\pi\phi_{HF}^0}{2} \right). \quad (39)$$

Initialization of MF parameters R_1 , Q_1 , ϕ_1 and R_2 , Q_2 , ϕ_2 . To initialize the MF parameters, we subtract the LF and HF spectra from the original one using their initial values:

$$\bar{Z}_{MF}(\boldsymbol{\theta}_{MF}^0; \omega) \approx \bar{Z}_{eq}(\boldsymbol{\theta}; \omega) - \bar{Z}_{LF}(\boldsymbol{\theta}_{LF}^0; \omega) - \bar{Z}_{HF}(\boldsymbol{\theta}_{HF}^0; \omega). \quad (40)$$

We can then find two peak points of the MF spectra corresponding to two Zarks at their characteristic frequencies ω_{c1} and ω_{c2} , we use Eq. (31) and (32) to initialize the parameters:

$$R_1^0 = 2 \cdot \Re(\bar{Z}_{MF}(\boldsymbol{\theta}; \omega_{c1})) \quad \text{and} \quad \phi_1^0 = \frac{4}{\pi} \arctan\left(-\frac{2\Im(\bar{Z}_{MF}(\boldsymbol{\theta}; \omega_{c1}))}{R_1^0}\right) \quad (41)$$

and similarly

$$R_2^0 = 2 \cdot (\Re(\bar{Z}_{MF}(\boldsymbol{\theta}; \omega_{c2})) - R_1^0) \quad \text{and} \quad \phi_2^0 = \frac{4}{\pi} \arctan\left(-\frac{2\Im(\bar{Z}_{MF}(\boldsymbol{\theta}; \omega_{c2}))}{R_2^0}\right). \quad (42)$$

The remaining parameters Q_1 and Q_2 can be initialized by expressing them from (27):

$$Q_1^0 = \frac{1}{(\omega_{c1})^{\phi_1^0} R_1^0} \quad \text{and} \quad Q_2^0 = \frac{1}{(\omega_{c2})^{\phi_2^0} R_2^0}. \quad (43)$$

2.7 General Gaussian CRLB for Estimated ECM Parameters

This section assesses the CRLB to find and compute the best possible CNLS estimator's variance. Since, in polar and Cartesian coordinates, the covariance matrix can be expressed as a function of parameters, $\mathbf{Q}(\boldsymbol{\theta}) = \text{diag}(\mathbf{Q}_1(\boldsymbol{\theta}), \dots, \mathbf{Q}_N(\boldsymbol{\theta}))$, a general Gaussian CRLB can be derived.

First, we assume that the probability density function of measurement mismatches is normal. I.e., the probability density function is given by the following expression:

$$p.d.f(\tilde{\mathbf{Z}}|\boldsymbol{\theta}, \boldsymbol{\omega}) = \frac{1}{\sqrt{(2\pi)^N \det \mathbf{Q}(\boldsymbol{\theta})}} \exp \left[-\frac{1}{2} \boldsymbol{\varepsilon}^\top(\boldsymbol{\theta}, \boldsymbol{\omega}) \mathbf{Q}^{-1}(\boldsymbol{\theta}) \boldsymbol{\varepsilon}(\boldsymbol{\theta}, \boldsymbol{\omega}) \right], \quad (44)$$

where $\boldsymbol{\varepsilon}(\boldsymbol{\theta}, \boldsymbol{\omega}) = \tilde{\mathbf{Z}}(\boldsymbol{\omega}) - \mathbf{Z}(\boldsymbol{\theta}, \boldsymbol{\omega})$ is the vector containing mismatches between the measurements and model function at frequencies $\boldsymbol{\omega}$. This enables us to find the Log-likelihood function L , expressed as follows:

$$L(\boldsymbol{\theta}, \boldsymbol{\omega}|\tilde{\mathbf{Z}}) = \ln p.d.f(\tilde{\mathbf{Z}}|\boldsymbol{\theta}) \quad (45)$$

$$L(\boldsymbol{\theta}, \boldsymbol{\omega}|\tilde{\mathbf{Z}}) = -\frac{N}{2} \ln 2\pi - \frac{1}{2} \ln \det \mathbf{Q}(\boldsymbol{\theta}) - \frac{1}{2} \boldsymbol{\varepsilon}^\top(\boldsymbol{\theta}, \boldsymbol{\omega}) \mathbf{Q}^{-1}(\boldsymbol{\theta}) \boldsymbol{\varepsilon}(\boldsymbol{\theta}, \boldsymbol{\omega}) \quad (46)$$

and to compute its first-order partial derivatives with respect to every parameter θ_j , $j = 1, \dots, M$:

$$\begin{aligned} \frac{\partial L(\boldsymbol{\theta}, \boldsymbol{\omega}|\tilde{\mathbf{Z}})}{\partial \theta_j} &= -\frac{1}{2} \frac{\partial}{\partial \theta_j} \ln \det \mathbf{Q}(\boldsymbol{\theta}) - \frac{1}{2} \frac{\partial}{\partial \theta_j} (\boldsymbol{\varepsilon}^\top(\boldsymbol{\theta}, \boldsymbol{\omega}) \mathbf{Q}^{-1}(\boldsymbol{\theta})) \\ &= -\frac{1}{2} \text{tr} \left(\mathbf{Q}^{-1}(\boldsymbol{\theta}) \frac{\partial \mathbf{Q}(\boldsymbol{\theta})}{\partial \theta_k} \right) + \frac{\partial \mathbf{Z}^\top(\boldsymbol{\theta}, \boldsymbol{\omega})}{\partial \theta_k} \mathbf{Q}^{-1}(\boldsymbol{\theta}) \boldsymbol{\varepsilon}(\boldsymbol{\theta}, \boldsymbol{\omega}) - \frac{1}{2} \boldsymbol{\varepsilon}^\top(\boldsymbol{\theta}, \boldsymbol{\omega}) \frac{\partial \mathbf{Q}(\boldsymbol{\theta})}{\partial \theta_k} \boldsymbol{\varepsilon}(\boldsymbol{\theta}, \boldsymbol{\omega}). \end{aligned}$$

The (k, l) -th element of the FIM, $\mathcal{F} \in \mathbb{R}^{M \times M}$, as a function of parameter vector $\boldsymbol{\theta}$ and angular frequency $\boldsymbol{\omega}$, is equal to the expected value of the product between partial derivatives of the Log-likelihood function with respect to k -th and l -th parameter:

$$\mathcal{F}_{k,l}(\boldsymbol{\theta}, \boldsymbol{\omega}) = \mathbb{E} \left[\frac{\partial L(\boldsymbol{\theta}, \boldsymbol{\omega}|\tilde{\mathbf{Z}})}{\partial \theta_k} \frac{\partial L(\boldsymbol{\theta}, \boldsymbol{\omega}|\tilde{\mathbf{Z}})}{\partial \theta_l} \right]. \quad (47)$$

The expression for (k, l) -th element of the FIM can be written in compact form as follows [28]:

$$[\mathcal{F}(\boldsymbol{\theta}, \boldsymbol{\omega})]_{k,l} = \frac{\partial \mathbf{Z}^\top(\boldsymbol{\theta}, \boldsymbol{\omega})}{\partial \theta_k} \mathbf{Q}^{-1}(\boldsymbol{\theta}) \frac{\partial \mathbf{Z}(\boldsymbol{\theta}, \boldsymbol{\omega})}{\partial \theta_l} + \frac{1}{2} \text{tr} \left(\mathbf{Q}^{-1}(\boldsymbol{\theta}) \cdot \frac{\partial \mathbf{Q}(\boldsymbol{\theta})}{\partial \theta_k} \cdot \mathbf{Q}^{-1}(\boldsymbol{\theta}) \cdot \frac{\partial \mathbf{Q}(\boldsymbol{\theta})}{\partial \theta_l} \right). \quad (48)$$

Measurements at different frequencies, in general, contribute differently to the elements of the FIM. Thanks to the fact that in Cartesian and polar coordinates, the covariance matrix is purely and block diagonal, respectively, it is possible to define the contribution to the FIM element (k, l) as a function of parameters $\boldsymbol{\theta}$ and frequency ω_i :

$$[\Delta \mathcal{F}_i(\boldsymbol{\theta})]_{k,l} = \frac{\partial z_i^\top(\boldsymbol{\theta})}{\partial \theta_k} \mathbf{Q}_i^{-1}(\boldsymbol{\theta}) \frac{\partial z_i(\boldsymbol{\theta})}{\partial \theta_l} + \frac{1}{2} \text{tr} \left(\mathbf{Q}_i^{-1}(\boldsymbol{\theta}) \cdot \frac{\partial \mathbf{Q}_i(\boldsymbol{\theta})}{\partial \theta_k} \cdot \mathbf{Q}_i^{-1}(\boldsymbol{\theta}) \cdot \frac{\partial \mathbf{Q}_i(\boldsymbol{\theta})}{\partial \theta_l} \right). \quad (49)$$

To calculate (k, l) element of \mathcal{F} , we can use the following property.

Property 1. The element (k, l) of the FIM can be expressed as a sum of contributions at every frequency ω_i , $i = 1, \dots, N$:

$$[\mathcal{F}(\boldsymbol{\theta}, \boldsymbol{\omega})]_{k,l} = \sum_{i=1}^N [\Delta \mathcal{F}_i(\boldsymbol{\theta})]_{k,l}. \quad (50)$$

When expressed in Cartesian coordinates, the vector $z_i(\boldsymbol{\theta})$ from (49) is $z_i(\boldsymbol{\theta}) = [R_i(\boldsymbol{\theta}), X_i(\boldsymbol{\theta})]^\top$ and $\mathbf{Q}_i(\boldsymbol{\theta})$ is a covariance matrix block:

$$\mathbf{Q}_i(\boldsymbol{\theta}) = \begin{bmatrix} \sigma^2(R_i(\boldsymbol{\theta})) & \sigma(R_i(\boldsymbol{\theta}), X_i(\boldsymbol{\theta})) \\ \sigma(R_i(\boldsymbol{\theta}), X_i(\boldsymbol{\theta})) & \sigma^2(X_i(\boldsymbol{\theta})) \end{bmatrix} = \begin{bmatrix} \alpha_i(\boldsymbol{\theta}) & \beta_i(\boldsymbol{\theta}) \\ \beta_i(\boldsymbol{\theta}) & \gamma_i(\boldsymbol{\theta}) \end{bmatrix}, \quad (51)$$

whose elements are expressed in terms of *true* values of the impedance (magnitude ρ_i and phase φ_i):

$$\alpha_i(\boldsymbol{\theta}) = \rho_i^2 e^{-\sigma_\varphi^2} [\cos^2 \varphi_i (\cosh(\sigma_\varphi^2) - 1) + \sin^2 \varphi_i \sinh(\sigma_\varphi^2)] \quad (52)$$

$$+ \sigma_{\rho_i}^2 e^{-\sigma_\varphi^2} [\cos^2 \varphi_i \cosh(\sigma_\varphi^2) + \sin^2 \varphi_i \sinh(\sigma_\varphi^2)]$$

$$\beta_i(\boldsymbol{\theta}) = \rho_i^2 e^{-\sigma_\varphi^2} [\sin^2 \varphi_i (\cosh(\sigma_\varphi^2) - 1) + \cos^2 \varphi_i \sinh(\sigma_\varphi^2)] \quad (53)$$

$$+ \sigma_{\rho_i}^2 e^{-\sigma_\varphi^2} [\sin^2 \varphi_i \cosh(\sigma_\varphi^2) + \cos^2 \varphi_i \sinh(\sigma_\varphi^2)]$$

$$\gamma_i(\boldsymbol{\theta}) = \sin \varphi_i \cos \varphi_i e^{-2\sigma_\varphi^2} [\sigma_{\rho_i}^2 + \rho_i^2 (1 - e^{\sigma_\varphi^2})]. \quad (54)$$

Note that $\rho_i = \rho_i(\boldsymbol{\theta})$, $\varphi_i = \varphi_i(\boldsymbol{\theta})$, $\sigma_{\rho_i} = \sigma_{\rho_i}(\boldsymbol{\theta})$ and $\sigma_\varphi = \text{const.}$

On the other hand, in polar coordinates $z_i(\boldsymbol{\theta}) = [\rho_i(\boldsymbol{\theta}), \varphi_i(\boldsymbol{\theta})]^\top$ and covariance matrix block is of a diagonal form:

$$\mathbf{Q}_i(\boldsymbol{\theta}) = \begin{bmatrix} \sigma_{\rho_i}^2(\boldsymbol{\theta}) & 0 \\ 0 & \sigma_\varphi^2 \end{bmatrix}. \quad (55)$$

Using either the polar or Cartesian coordinates, the calculation of the CRLB requires the evaluation of the FIM elements at the true parameter values, $\boldsymbol{\theta}_{\text{true}}$, which are unknown in practice:

$$[\mathcal{F}]_{k,l} = [\mathcal{F}(\boldsymbol{\theta}, \boldsymbol{\omega})]_{k,l} \Big|_{\boldsymbol{\theta} = \boldsymbol{\theta}_{\text{true}}}. \quad (56)$$

The diagonal elements of the FIM inverse, $\mathbf{C} \triangleq \mathcal{F}^{-1}$, evaluated at parameters' true values and frequency values, provide CRLB for each parameter and define the least possible variance of the estimated parameter. Namely:

$$\sigma_{\theta_i}^2 \triangleq \text{Var}(\theta_i) \geq \mathbf{C}_{i,i}, \quad \forall i = 1, \dots, M. \quad (57)$$

2.8 Least-variance Circuit Parameter Identification via CRLB

When performing EIS measurements, it is common to use logarithmically spaced frequency points, say N , from a minimum f_{min} to a maximum f_{max} desired frequency to measure the cell's impedance.

As known from classical information theory, we expect that different circuit parameters are dominant at different frequency ranges, i.e. different parameters achieve a maximum contribution to the FIM at different frequencies (see Fig. 4 of Section 3.1.3). Therefore, for a fixed single frequency point, each parameter contributes differently to the FIM. Modifying such frequency affects the variances of all estimated parameters and justifies the search for frequencies that improve the overall estimation accuracy.

For the multi-parameter estimation problem where all the parameters are mutually coupled, there exist different techniques one can use to improve the FIM and, consequently, minimize the variances of the estimates. Some of these include maximizing: the trace of FIM, the determinant of FIM, and the smallest eigenvalue of FIM, known as A-, D- and E-optimal experiment design, respectively.

In this section, we propose an algorithm to find a set of frequencies that provide measurements carrying the most information to estimate ECM parameters by maximizing the smallest eigenvalue of the FIM.

2.9 E-optimal design

The square FIM, \mathcal{F} , is a real, symmetric, positive-semidefinite matrix. Therefore, it has M real and non-negative eigenvalues. Let's define the M -dimensional vector of the FIM's eigenvalues as

$$\Lambda = [\lambda_1, \dots, \lambda_M]^\top \in \mathbb{R}^M \quad (58)$$

with eigenvalues in non-descending order $0 \leq \lambda_1 \leq \dots \leq \lambda_M$.

The eigenvalues of the FIM's inverse \mathcal{C} are equal to the reciprocal values of the eigenvalues of the FIM \mathcal{F} . Therefore, the eigenvalues of \mathcal{C} are

$$\frac{1}{\lambda_1}, \dots, \frac{1}{\lambda_M} \text{ with } \frac{1}{\lambda_1} \geq \dots \geq \frac{1}{\lambda_M} \geq 0. \quad (59)$$

As known, square roots of eigenvalues of FIM's inverse, $\mathcal{C} = \mathcal{F}^{-1}$, represent the length of semi-axes of estimated parameters' confidence ellipsoid [29]. Since the smallest eigenvalue of \mathcal{F} defines the highest eigenvalue of \mathcal{C} , to minimize the length $\sqrt{1/\lambda_1}$ of the largest semi-axis of the confidence ellipsoid, it is sufficient to maximize the smallest eigenvalue of the \mathcal{F} matrix, λ_1 . We will show that it consequently results in a decrease of the volume of M -dimensional confidence ellipsoid given by:

$$V_M = \frac{2}{M} \frac{\pi^{\frac{M}{2}}}{\Gamma(\frac{M}{2})} \prod_{i=1}^M \sqrt{1/\lambda_i}, \quad (60)$$

where Γ is the gamma function [30]. It is worth mentioning that we neglect the exact correspondence between eigenvalues and parameters but focus on minimizing the largest axis of the confidence ellipsoid to improve the overall accuracy.

2.10 Algorithm: Frequencies Adjustments via E-optimal Design

The proposed algorithm's objective is to adjust the initial set of frequencies so that the new frequency set provides better estimates than the traditional log-spaced frequency span. The initial and final set of frequencies will have the same predetermined number of points, N and the frequency range $[f_{min}, f_{max}]$. With $\Omega = \{1, 2, \dots, N\}$, we denote the set of indices of frequency measurement points.

Algorithm 2 Frequencies Adjustments via E-optimal Design

```

1: Initialize  $k = 0$ ,  $\Omega = \{1, \dots, N\}$ ,  $\Omega_c = \emptyset$ ,  $f_{min}$ ,  $f_{max}$ ,  $\kappa$ 
2: do
3:   if  $k = 0$  then
4:      $\omega^k = \text{logspace}(2\pi f_{min}, 2\pi f_{max}, N)$ 
5:     Obtain  $\tilde{Z}(\omega^k) = [\tilde{Z}(\omega_1^k), \dots, \tilde{Z}(\omega_N^k)]^\top$ 
6:      $\theta_{init} \leftarrow \theta_0$  (from the procedure described in Sec. 2.6)
7:   else
8:      $\omega^k \leftarrow \omega^{k-1}$ 
9:     Obtain only  $\tilde{Z}(\omega_m^k)$ 
10:    Update:  $\tilde{Z}(\omega^k) \leftarrow [\tilde{Z}(\omega_1^{k-1}), \dots, \tilde{Z}(\omega_m^k), \dots, \tilde{Z}(\omega_N^{k-1})]^\top$ 
11:     $\theta_{init} \leftarrow \hat{\theta}^{k-1}$ 
12:   end if
13:   Estimate the ECM parameters,  $\hat{\theta}^k$  by solving (3) with initial guess  $\theta_{init}$ 
14:   Compute FIM:  $\mathcal{F}^k = \text{FIM}(\omega^k, \hat{\theta})$  using (48)
15:   Compute eigenvalues of FIM:  $\Lambda^k = \text{eig}(\mathcal{F}^k) = [\lambda_1^k, \dots, \lambda_M^k]^\top$ 
16:   for  $i \in \Omega \setminus \Omega_c$  do
17:      $\Delta\omega_i^k = \frac{\omega_i^k}{\kappa}$ 
18:     if  $i = N$  then
19:        $\omega_i^k \leftarrow \omega_i^k - \Delta\omega_i^k$ 
20:     else
21:        $\omega_i^k \leftarrow \omega_i^k + \Delta\omega_i^k$ 
22:     end if
23:      $\mathcal{F}_{\Delta i}^k = \text{FIM}(\omega^k, \hat{\theta})$ 
24:      $\Lambda_{\Delta i}^k = \text{eig}(\mathcal{F}_{\Delta i}^k)$ 
25:      $d_i^k = \frac{\min \Lambda^k - \min \Lambda_{\Delta i}^k}{\Delta\omega_i^k}$ 
26:   end for
27:    $d_m^k = \text{argmax}_{d_i^k} \{|d_i^k| : i \in \Omega \setminus \Omega_c\}$ 
28:    $s = \text{sgn}(d_m^k)$ 
29:    $n \leftarrow 1$ 
30:   do
31:      $\omega_m^k \leftarrow \omega_m^k + s \cdot n \Delta\omega_m^k$ 
32:     if  $\omega_m^k \geq 2\pi f_{max}$  or  $\omega_m^k \leq 2\pi f_{min}$  then
33:        $\omega_m^k \leftarrow 2\pi [(s-1)f_{min} + (1-s)f_{max}]$ 
34:     break
35:   end if
36:    $\mathcal{F}_{n\Delta m}^k = \text{FIM}(\omega^k, \hat{\theta})$ 
37:    $\Lambda_{n\Delta m}^k = \text{eig}(\mathcal{F}_{n\Delta m}^k)$ 
38:    $n \leftarrow n + 1$ 
39:   while  $\min \Lambda_{n\Delta m}^k > \min \Lambda_{(n-1)\Delta m}^k$ 
40:    $\omega_m^k \leftarrow \omega_m^k + s \cdot (n-1) \Delta\omega_m^k$ 
41:    $\Omega_c \leftarrow \Omega_c \cup \{m\}$ 
42:    $k \leftarrow k + 1$ 
43: while  $\Omega_c \neq \Omega$ 

```

Globally, the algorithm's iterations consist of the following main parts: perform the EIS measurements at defined frequencies (lines 3-12), estimating the ECM parameters, FIM and its eigenvalues (lines 13-15), decide which frequency to adjust (lines 16-28) and optimally adjust it using a gradient approach (lines 29-41). The algorithm terminates when adjustments of all the frequencies are identified and implemented.

The first stage (line 1) initializes the iteration counter k , the set of frequency measurements'

indices Ω and the set of already adjusted and fixed frequencies, Ω_c . As input, the user defines the minimum and maximum frequencies for the EIS measurements, f_{min} and f_{max} , and the parameter κ , used to numerically compute small perturbations of the frequencies through the iterations.

In the preliminary iteration (for $k = 0$) the modeller can use N frequency points spread logarithmically between defined frequency bounds and obtain N impedance measurements. ECM parameters can be initialized by applying the described procedure in Section 2.6, $\theta_{init} = \theta_0$. In all the other iterations, the impedance is measured only at the frequency adjusted in the previous iteration. ECM parameters take the initial values equal to the estimated ones from the previous iteration, $\theta_{init} = \hat{\theta}^{k-1}$. On estimating the ECM parameters, we compute the FIM calculated using the estimated parameters' values and find its eigenvalues using the procedures `FIM` and `eig`.

The lines 16-28 of the pseudo-code decide which frequency to adjust (from the set of frequencies that have not been adjusted). It finds the index of the frequency for which adjustment has the most impact on the minimum eigenvalue of the FIM. This step is done numerically: the algorithm perturbs each candidate frequency ω_i , $i \in \Omega \setminus \Omega_c$, one by one, by increasing it by its small fraction, $\Delta\omega_i$. To satisfy the pre-determined frequency bounds f_{min} and f_{max} , the highest frequency point, ω_N is decreased by $\Delta\omega_i$ and we assume that κ is chosen such that for all the other frequencies, $\Delta\omega_i$ is sufficiently small so that the perturbed frequency stays within the bounds. In that case, one should ensure:

$$\omega_{N-1} + \Delta\omega_{N-1} = \omega_{N-1} + \frac{\omega_{N-1}}{\kappa} \leq 2\pi f_{max}, \quad (61)$$

and therefore

$$\kappa \geq \frac{\omega_{N-1}}{2\pi f_{max} - \omega_{N-1}}. \quad (62)$$

The FIM and its eigenvalues are re-computed for each perturbation. In k -th iteration, the metric used to quantify the impact of the perturbation of ω_i on the minimum eigenvalue of the FIM, is denoted as d_i^k . It represents a sensitivity of the minimum eigenvalue of the FIM to the perturbation of frequency ω_i . By finding the maximum sensitivity (by the absolute value, since d_i^k can also take negative values), the algorithm decides the index of the best suitable frequency to adjust and the direction of the adjustment (i.e., depending on the sign of the sensitivity).

In lines 29-41 of the pseudo-code, the algorithm further perturbs the chosen frequency (index denoted as m) in discreet steps by multiplying $\Delta\omega_m^k$ by the loop counter n and the sensitivity sign s . In case the frequency bounds are violated, by increasing or decreasing the frequency, the algorithm fixes the current frequency to the maximum or minimum frequency, respectively (lines 32-35). It then re-computes the FIM and its eigenvalues until there is no further improvement (increase) of the minimum eigenvalue. Therefore, the frequency point is considered to be adjusted and fixed. Its index is then included in the set of already adjusted frequencies Ω_c . The algorithm terminates when all the frequencies are adjusted.

3 Results and Discussion

This section presents the results of numerical simulations and a dedicated experimental validation carried out on a real Li-ion cell used to verify the proposed methods for parameter initialization, estimation, accuracy assessment and frequency adjustment.

3.1 Numerical Simulations

The main advantage of performing a numerical simulation is the knowledge of the parameters' true values, which are always unknown in practice. In what follows, we generate synthetic, noisy EIS measurements using the chosen ECM topology with known parameters and respecting the measurement model. We use this data to validate the proposed methodology presented in Section 2.

3.1.1 Cell and Measurement Model

Circuit Topology. We use the ECM for the Li-ion battery cell shown in Fig. 1. The parameter vector is:

$$\boldsymbol{\theta} = [R_s, Q_{HF}, \phi_{HF}, R_1, Q_1, \phi_1, R_2, Q_2, \phi_2, Q_W]^\top. \quad (63)$$

For simulation purposes, we assume to know the ECM parameters' *true values*, listed in Tab. 1. **Impedance Data Generation.** Artificial EIS measurements are generated by assuming that the topology and true values of the Full Randles ECM parameters are known and equal to $\boldsymbol{\theta}_{\text{true}}$. The measurement errors follow Gaussian distribution according to the discussed measurement model from Sec. 2.2, with relative error in magnitude $\varepsilon_\rho = 1\%$ and absolute error in phase $\varepsilon_\varphi = 1^\circ$ (these values are quite typical for commercial EIS spectrometers). Therefore, here we assumed that our EIS measurements belong within a unique accuracy contour. The following pseudo-code describes the generation of noisy impedance measurements within a specific accuracy contour plot.

Algorithm 3 EIS Data Generation

```

1: Initialize  $\boldsymbol{\omega}$ ,  $\boldsymbol{\theta}_{\text{true}}$ , ECM topology,  $\varepsilon_\rho$ ,  $\varepsilon_\varphi$ 
2: for  $i = 1 : N$  do
3:    $R_i = R_i(\boldsymbol{\theta}_{\text{true}})$ ,  $X_i = X_i(\boldsymbol{\theta}_{\text{true}})$ 
4:    $Z_i = R_i + jX_i$ 
5:    $\rho_i = |Z_i|$ ,  $\varphi_i = \arg(Z_i)$ 
6:    $\Delta\rho \leftarrow \mathcal{N}(0, \frac{\rho_i \varepsilon_\rho}{3})$ 
7:    $\Delta\varphi \leftarrow \mathcal{N}(0, \frac{\varepsilon_\varphi}{3})$ 
8:    $\tilde{\rho}_i = \rho_i + \Delta\rho$ 
9:    $\tilde{\varphi}_i = \varphi_i + \Delta\varphi$ 
10:   $\tilde{Z}_i = \tilde{\rho}_i e^{j\tilde{\varphi}_i}$ 
11:   $\tilde{R}_i = \Re(\tilde{Z}_i)$ ,  $\tilde{X}_i = \Im(\tilde{Z}_i)$ 
12: end for

```

It is important to mention that, according to the EIS instrument characteristics, the normal distribution of measurement errors is valid in polar coordinates for both magnitude and phase. After the projection from polar to Cartesian coordinates, residuals for the real and imaginary parts are, in general, no longer normally distributed. However, for considered values of $\varepsilon_\rho = 1\%$ and $\varepsilon_\varphi = 1^\circ$, after the projection, errors of the real and imaginary part are practically normal [27]. This is confirmed by comparing the quantile-quantile (QQ) plots for the noise of both real and imaginary parts of simulated impedance measurements (of a corresponding error structure) with the ones of a standard normal random variable. An interested reader can generate these QQ plots and easily verify this statement.

3.1.2 Parameters' Initial Guess and Fitted Values Accuracy

In what follows, we analyze the accuracy of the parameters' initial guess and fitted values after carrying out a controlled numerical experiment with known true values of the parameters. To show that the fitting algorithm provides the estimated values of the parameters close to the true values

with an expected accuracy, we performed 1000 simulations. In each simulation, we generate the noisy EIS data as described in Algorithm 3 for a logarithmically spread set of frequencies, from $f_{min} = 10^{-2}$ Hz to $f_{max} = 10^4$ Hz and 10 ppd. We set the frequency perturbation coefficient to $\kappa = 0.01$. All the ECM parameters are first initialized by applying the described process of Section 2.6.2 and then estimated by solving the optimization problem (5), in polar, and (9), in Cartesian coordinates. Tab. 2 shows the mean values of the parameters' initial guess after simulations. The proposed method for the initialization, where all ten parameters are initialized only by applying the properties of the EIS spectrum and before running the weighted CNLS fitting method, provides approximate values which do not exceed 16% for R_s , while most of the parameters are initialized with the accuracy better than 8%.

Param.	θ	μ_{θ_0}	$\left \frac{\theta - \theta_0}{\theta} \right \cdot 100$ (%)
R_s	3.800E-02	4.227E-02	15.90
Q_{HF}	1.667E+04	1.736E+04	7.53
ϕ_{HF}	-8.500E-01	-8.519E-01	0.70
R_1	4.500E-01	4.714E-01	4.75
Q_1	2.000E-02	1.815E-02	10.44
ϕ_1	9.000E-01	9.425E-01	4.72
R_2	6.500E-01	6.382E-01	1.90
Q_2	4.000E-01	3.593E-01	12.38
ϕ_2	9.000E-01	9.425E-01	4.72
Q_W	3.693E+00	3.537E+00	4.24

Table 2: True and initial ECM parameters' values.

The CNLS estimation results are presented in Tab. 3. Both formulations in polar and Cartesian coordinates provide the same results. The mean value $\mu_{\hat{\theta}}$ of each estimated parameter is extremely close to its true value (maximum relative error of 1.134% for Q_{HF}). Therefore, our estimator is unbiased. We calculated the variance of each parameter from the collection of all the estimated parameters' values. On the other hand, by having access to the parameters' true values, we computed the CRLB, defining the best possible variance of estimated parameters for an unbiased estimator. The calculated variance from 1000 simulations is quite close to the exact CRLB for the first nine parameters. This variance is slightly lower for the Q_W , due to the finite number of repeated simulations. However, the results indicate that our estimator is efficient, i.e., the estimator is capable of attaining the CRLB.

Param.	θ	$\mu_{\hat{\theta}}$	$\left \frac{\theta - \mu_{\hat{\theta}}}{\theta} \right $	$\sigma_{\hat{\theta}}^2$	CRLB $_{\theta}$	$\frac{\sigma_{\hat{\theta}}^2}{\theta^2}$	$\frac{\text{CRLB}_{\theta}}{\theta^2}$
R_s	3.800E-02	3.801E-02	0.752%	1.279E-07	1.159E-07	8.860E-03	8.028E-03
Q_{HF}	1.667E+04	1.668E+04	1.134%	5.602E+04	5.065E+04	2.017E-02	1.823E-02
ϕ_{HF}	-8.500E-01	-8.500E-01	0.129%	1.902E-06	1.723E-06	2.633E-04	2.385E-04
R_1	4.500E-01	4.499E-01	0.476%	7.220E-06	6.860E-06	3.565E-03	3.388E-03
Q_1	2.000E-02	1.999E-02	0.956%	5.743E-08	5.335E-08	1.436E-02	1.334E-02
ϕ_1	9.000E-01	9.001E-01	0.201%	5.075E-06	4.666E-06	6.266E-04	5.761E-04
R_2	6.500E-01	6.502E-01	0.652%	2.806E-05	2.788E-05	6.641E-03	6.599E-03
Q_2	4.000E-01	4.000E-01	0.585%	8.788E-06	8.710E-06	5.492E-03	5.444E-03
ϕ_2	9.000E-01	8.999E-01	0.484%	2.965E-05	2.921E-05	3.660E-03	3.606E-03
Q_W	3.693E+00	3.693E+00	0.464%	4.560E-04	4.586E-04	3.344E-03	3.363E-03

Table 3: True and estimated ECM parameters' values and the estimation accuracy.

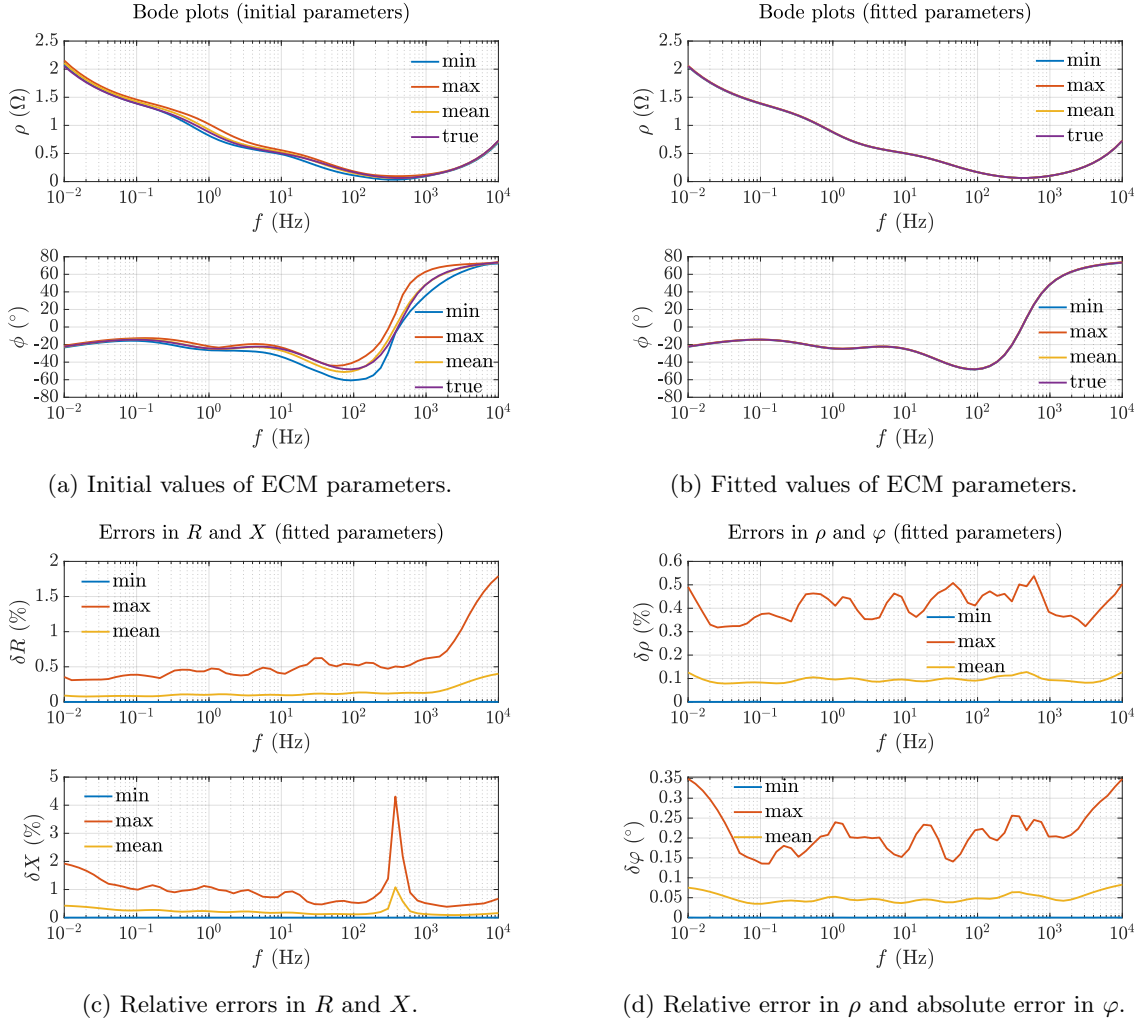


Figure 3: Bode plots obtained using the initial and estimated parameters (a-b) and minimum, maximum and mean errors of reconstructed EIS spectra compared to the true values (c-d).

To illustrate the accuracy of the initialized and estimated parameters' values, in each simulation, the EIS data is reconstructed by evaluating the equivalent impedance functions given by (19) and (20) at the obtained initial and estimated value for the defined frequency span. From the entire families of Bode curves, in Fig. 3a and Fig. 3b, we show the minimum, maximum, mean, and true value of the impedance magnitude and phase at a specific frequency, using the initial and fitted estimated parameters' values, respectively. Since the curves in Fig. 3b are extremely close, Fig. 3c and 3d show minimum, maximum and mean values of the errors in Cartesian and polar coordinates, respectively, from the reconstructed EIS data using the estimated values, with reference to the true EIS spectrum.

3.1.3 Parameters' Contributions to the FIM

Using the expression (49), for a certain frequency region, it is possible to show the evolution of different contributions to the FIM, as a function of frequency. In Fig. 4, the contributions to the diagonal elements of FIM are shown for the frequency range from $f_{min} = 10^{-2}$ Hz to $f_{max} = 10^4$ Hz. For visibility, each curve is normalized by its peak value achieved in this range.

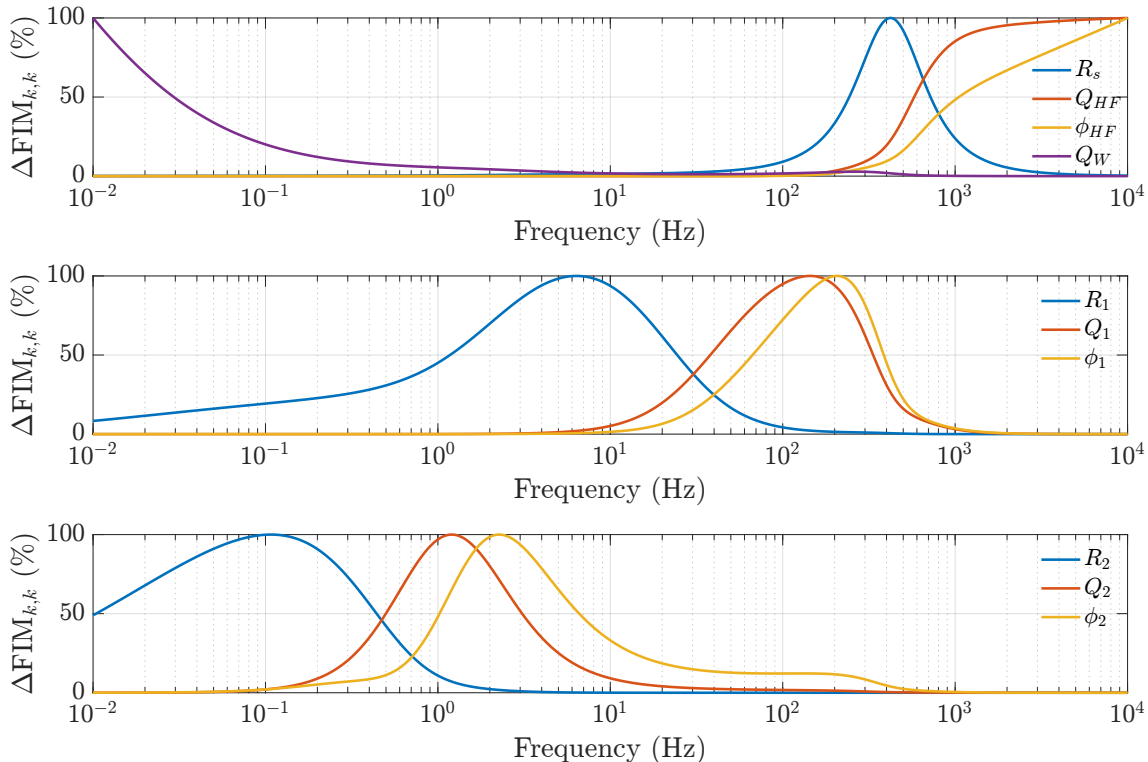


Figure 4: Contributions to the diagonal elements of FIM as a function of frequencies for every ECM parameter.

For different parameters, different frequencies provide measurements at which the diagonal elements of the FIM reach their peak values. As expected, contributions from the elements R_s and Q_{HF} and ϕ_{HF} are the highest at high frequencies, while from Q_W is increasing towards low frequencies. Peaks of the contribution curves corresponding to CPE1 parameters (R_1, Q_1, ϕ_1) and CPE2 (R_2, Q_2, ϕ_2) are within the mid-frequency region, in the expected order, having the time constants τ_1 and τ_2 where $\tau_1 < \tau_2$.

3.1.4 Parameters and Variances Identification

In this part, we present the results obtained after executing the proposed algorithm for frequency adjustment. The purpose of the numerical study is to compare the performance of the proposed algorithm for frequency adjustments and show that for that measurements at resulting frequencies convey more information than ones performed at log-spaced frequencies. Therefore the overall accuracy of parameters' estimated values increases.

Fig. 5 illustrates the adjustment of frequencies throughout the iterations. Frequencies with $i \in \Omega$, i.e., candidate frequencies, in the current iteration are shown in black dots. After perturbation of all candidate frequencies, the algorithm decides which frequency perturbation has the highest impact on the minimum eigenvalue of the FIM (i.e., as a result of lines 16-28 of the pseudo-code). At each iteration, this frequency is indicated as *considered frequency* and coloured in red. After the frequency is finally adjusted and fixed (i.e., as a result of lines 29-41 of the pseudo-code), it is indicated as a blue empty dot connected to its value in the previous iteration to track the change and level of adjustment.

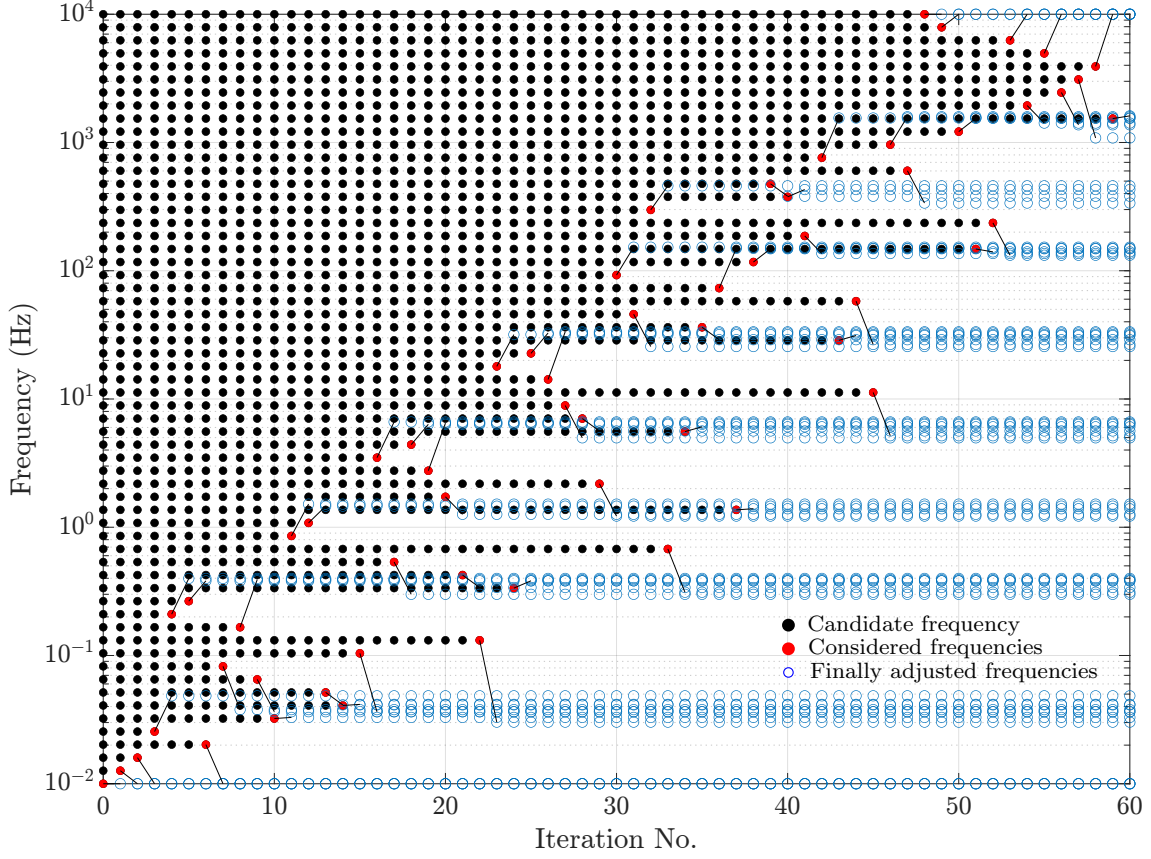


Figure 5: Frequencies adjustments via E-optimal design.

At each iteration, we compare true CRLB, calculated using the parameters' true values, θ with its approximate value, which is evaluated at the parameters' estimated values, at the current iteration, $\hat{\theta}$. Fig. 6 shows the evolution of the CRLB throughout the iterations, namely, $\mathcal{C}_{i,i}(\theta, \omega^k)$ and $\mathcal{C}_{i,i}(\hat{\theta}^k, \omega^k)$, $i = 1, \dots, M$ in a percentage of the CRLB at the log-spaced frequencies at the beginning of the algorithm. The CRLB for i -th parameter is computed by finding the i -th diagonal element of inverted FIM calculated using the expression (50). Note that all the decisions for frequency adjustment along the iterations are taken using the information about the FIM that is calculated using the estimated parameters' values. As the set of frequencies is being modified for most of the parameters, the CRLB is improving. For parameters θ_7, θ_8 and θ_9 , the CRLB at the final set of frequencies is slightly, but negligibly increased, by 0.70%, 1.71% and 0.05%, respectively. From the figure, we also conclude that by using the estimated parameters from each iteration to calculate the CRLB, the approximation is tracking well the true values.

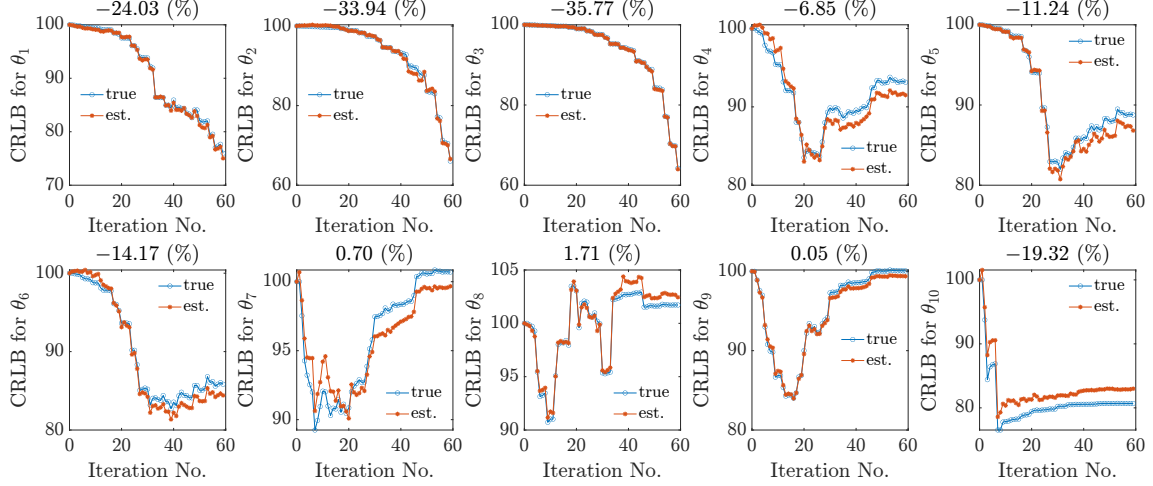


Figure 6: Relative improvement in CRLB for each ECM parameter compared to the initial log-spaced frequency span.

To quantify the overall improvement, in Fig. 7, we also show the evolution of the parameters confidence ellipsoid's volume (normalized with the true initial volume of the confidence ellipsoid) along the iterations, calculated using (60) and evaluated at both true and estimated parameters' values at each iteration. The frequency adjustment, while maximizing the lowest eigenvalue of the FIM and consequently minimizing the highest eigenvalue of its inverse, also reduces the volume of the confidence ellipse and improves the overall parameter estimation. After the termination of the algorithm, the confidence ellipsoid decreased in volume by at least 25%.

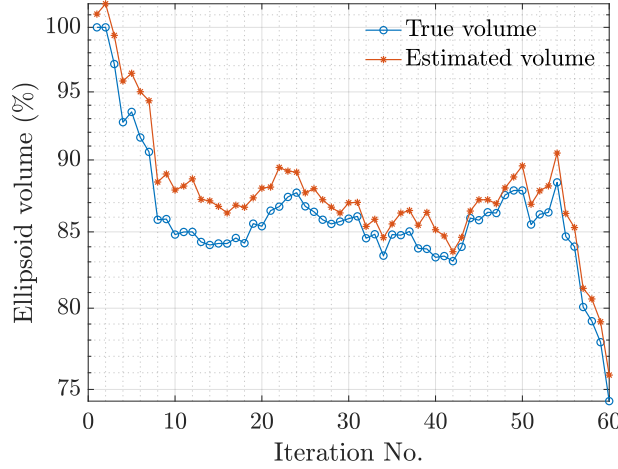


Figure 7: Evolution of the confidence ellipsoid volume while adjusting the frequencies along the algorithm's iterations.

3.2 Experimental Validation on Li-ion Cells

The proposed methods are experimentally validated on a Li-ion 5 Ah cell SLPB 11543140H5 by Kokam Ltd., in correspondence of two states of the cell: (a) 25 °C and 80% SoC and (b) at 15 °C and 20% SoC.

3.2.1 Experimental Setup

The cell is first brought to a certain SoC level by constant current constant voltage (CC-CV) charge/discharge to a corresponding voltage from the manufacturer OCV-SoC curve. We use a standard charging/discharging current of $C/5 = 1$ A. The cell is placed in a climatic chamber at a constant temperature. Before the measurements, the cell rests at a constant temperature for twelve hours to reach the equilibrium. We performed the EIS measurements in galvanostatic mode, exciting the cell with a small sinusoidal current with $\Delta I_{rms} = 0.5$ A (i.e., corresponding to a $C/10$ rate for the considered 5 Ah cell). We monitor the Lissajous figures at each frequency point, ensuring the cell is in the pseudo-linear regime. Initial EIS is done from $f_{max} = 10$ kHz to $f_{min} = 0.01$ Hz with 5 ppd. For frequency perturbations within the proposed algorithm, we set $\kappa = 0.01$.

3.2.2 Parameters and Variances Identification

The cell EIS response justifies using the ECM of the same structure already introduced and shown in Fig. 1. Since there is a slight deviation from the unity slope in the LF spectrum locus, the LF impedance is modelled with CPE(Q_{LF}, ϕ_{LF}) instead of pure Warburg impedance to improve the fitting. The LF CPE coefficient Q_{LF} is in $S \cdot s^{-\phi_{LF}}$. Hence, the parameter vector used for the experimental validation is

$$\theta = [R_s, Q_{HF}, \phi_{HF}, R_1, Q_1, \phi_1, R_2, Q_2, \phi_2, Q_{LF}, \phi_{LF}]^T. \quad (64)$$

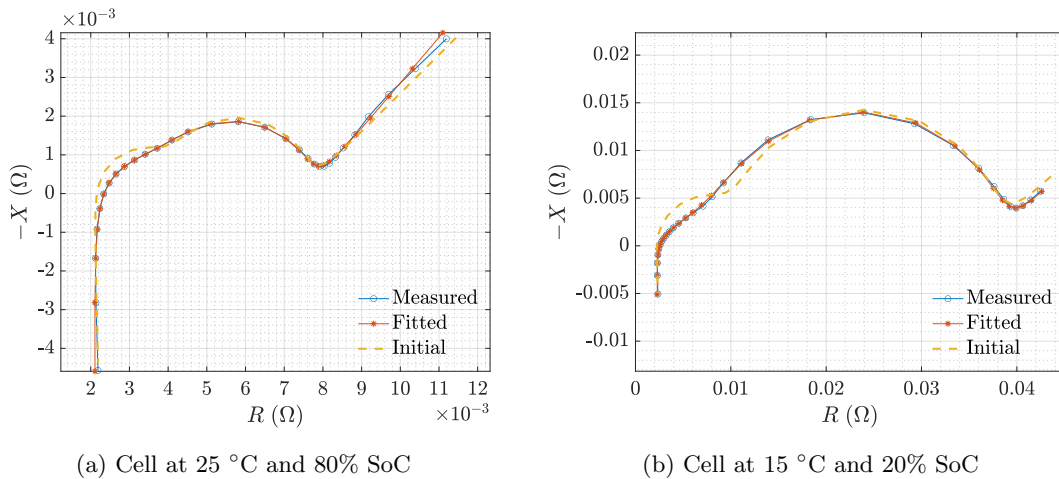


Figure 8: Measured impedance spectrum of Kokam SLPB 11543140H5 cell and reconstructed spectra using the initial and fitted parameters' values.

The parameter initialization is done by following the steps described in Sec. 2.6.2. Since the spectrum slope at LF is close to the unit slope, it is sufficient to initialize LF parameters as if ECM consisted of pure Warburg impedance and let the fitting adjust the parameters. As it can be observed from Fig. 8, the part of the spectrum at MF consists of two arcs. However, due to the high overlapping between them, it is not trivial to identify all the characteristic points. Therefore, from the MF spectrum (obtained by subtracting the influence of HF and LF spectrum), one can first initialize the more geometrically dominant arc, in this case, Zarc2. Once the parameters R_2, Q_2 and ϕ_2 are initialized, the remaining R_1 can be found as $R_1 = R_{\Sigma} - R_s - R_2$. The approximation for ω_{c1} can then be found from the MF spectrum point with the real part closest to $R_1/2$ and

the exponent ϕ_1 is sufficient to initialize with some typical values (e.g., $\phi_1 = 0.9$ or 1). Starting from the initial point, the CNLS algorithm finds the optimal fitting. Figures 8a and 8b show the obtained EIS spectra of a Kokam cell in two different states. They also show the reconstructed spectra, assuming the values of the parameters equal to the initial and fitted ones. The fitting matches the measurements quite well for both states, certifying the ECM choice and demonstrating the estimator's efficiency.

Tables 4 and 5 report the numerical results of the experimental validation of the proposed Algorithm 2 for frequencies adjustments via E-optimal design. They show the estimated ECM parameter values $\hat{\theta}_1$ at the beginning of the algorithm (i.e., from EIS measurements at logarithmically spread frequencies) and after final adjustment of the set of frequencies, $\hat{\theta}_N$ and the corresponding estimated CRLBs (absolute values and normalized values with respect to each estimated parameter squared). The last column shows the percentage improvement, i.e., the percentage change of the initial CRLB for every parameter. Negative values indicate a decrease in the CRLB. At 25 °C and 80% SoC parameters' CRLB improved by 16.4% on average, while at 15 °C and 20% SoC, the improvement is even more significant with 28.22%, on average. Fig. 9 shows the evolution of the volume of the confidence ellipsoids throughout iterations normalized with the volume at the beginning of the algorithm. At 25 °C and 80% SoC, the volume reduces by nearly 20%, while at 15 °C and 20% SoC, the decrease is even more significant, by 55%. This confirms that the frequency adjustments are parameter- and state-dependent. It is worth mentioning that the adjusted frequencies in every iteration can slightly differ from the ones provided by the algorithm due to the discreet frequency steps of the EIS measurement device's signal generator. I.e., the EIS measurement device measures at the nearest frequency to the value provided by the algorithm.

Param.	$\hat{\theta}_1$	$\hat{\theta}_N$	CRLB ₁	CRLB _N	$\frac{\text{CRLB}_1}{\hat{\theta}_1^2}$	$\frac{\text{CRLB}_N}{\hat{\theta}_N^2}$	ΔCRLB (%)
R_s	1.937E-03	1.936E-03	1.698E-09	1.257E-09	4.527E-04	3.351E-04	-25.99
Q_{HF}	1.132E+07	1.132E+07	5.683E+11	4.113E+11	4.431E-03	3.208E-03	-27.61
ϕ_1	-9.845E-01	-9.842E-01	3.502E-05	2.516E-05	3.613E-05	2.596E-05	-28.16
R_1	2.409E-03	2.393E-03	6.146E-08	4.834E-08	1.059E-02	8.333E-03	-21.34
Q_1	4.715E+00	4.622E+00	8.381E-01	6.344E-01	3.771E-02	2.854E-02	-24.31
ϕ_1	6.618E-01	6.631E-01	8.927E-04	6.856E-04	2.038E-03	1.566E-03	-23.20
R_2	3.273E-03	3.385E-03	4.504E-08	3.762E-08	4.205E-03	3.512E-03	-16.47
Q_2	6.419E+00	6.409E+00	4.802E-02	4.011E-02	1.165E-03	9.733E-04	-16.49
ϕ_2	9.347E-01	9.306E-01	3.161E-04	2.911E-04	3.617E-04	3.332E-04	-7.90
Q_{LF}	8.585E+02	8.845E+02	1.881E+02	2.025E+02	2.552E-04	2.748E-04	+7.66
ϕ_{LF}	5.553E-01	5.656E-01	3.447E-05	3.569E-05	1.118E-04	1.157E-04	+3.53

Table 4: Numerical results for Kokam cell at 25 °C and 80% SoC: parameters' estimated values, estimated CRLBs in the first and last iteration of optimal frequency adjustment algorithm and CRLB percentage improvement.

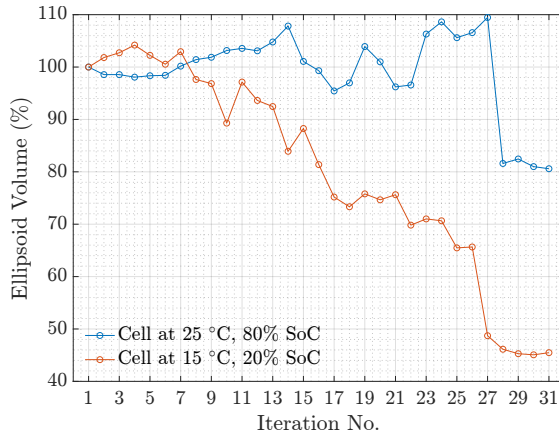


Figure 9: Evolution of the estimated confidence ellipsoid volume for two different cell states.

Param.	$\hat{\theta}_1$	$\hat{\theta}_N$	CRLB ₁	CRLB _N	$\frac{\text{CRLB}_1}{\hat{\theta}_1^2}$	$\frac{\text{CRLB}_N}{\hat{\theta}_N^2}$	ΔCRLB (%)
R_s	2.017E-03	2.095E-03	6.343E-10	4.123E-10	1.559E-04	1.013E-04	-34.99
Q_{HF}	1.020E+07	1.082E+07	2.137E+11	1.587E+11	2.056E-03	1.527E-03	-25.71
ϕ_1	-9.849E-01	-9.899E-01	1.719E-05	1.126E-05	1.772E-05	1.161E-05	-34.48
R_1	9.535E-03	7.804E-03	2.637E-07	1.009E-07	2.901E-03	1.110E-03	-61.74
Q_1	8.307E+00	6.767E+00	2.097E-01	1.172E-01	3.039E-03	1.698E-03	-44.13
ϕ_1	5.698E-01	6.029E-01	8.329E-05	6.815E-05	2.566E-04	2.099E-04	-18.18
R_2	2.647E-02	2.800E-02	3.147E-07	2.034E-07	4.493E-04	2.904E-04	-35.37
Q_2	6.497E+00	6.227E+00	7.280E-03	3.536E-03	1.724E-04	8.375E-05	-51.43
ϕ_2	9.546E-01	9.363E-01	5.879E-05	4.520E-05	6.452E-05	4.960E-05	-23.12
Q_{LF}	6.250E+02	6.233E+02	3.280E+03	3.626E+03	8.399E-03	9.284E-03	+10.53
ϕ_{LF}	5.356E-01	5.368E-01	7.495E-04	8.108E-04	2.612E-03	2.826E-03	+8.18

Table 5: Numerical results for Kokam cell at 15 °C and 20% SoC: parameters’ estimated values, estimated CRLBs in the first and last iteration of optimal frequency adjustment algorithm and CRLB percentage improvement.

4 Conclusion

In this paper, we presented a rigorous formulation of the ECM parameters identification problem for Li-ion batteries from EIS measurements. We developed the method to initialize the parameters of one of the most complete ECMs containing ten parameters. This automated method can be implemented into EIS measuring device software to help users run the CNLS method with a good starting point. We then studied and derived general CRLB applied to this specific identification problem, enabling us to design the experiments by quantifying the best possible accuracy of the parameter estimates. Since these values are highly dependent on the frequency set at which the EIS measurements are done, we developed the algorithm that modifies the initial logarithmic frequency span used for EIS measurements. This is done by utilizing the FIM and maximizing its lowest eigenvalue via the E-optimal design. In the numerical study, where we assumed the true parameters’ values to be known, we showed that the variances for most of the ECM parameters were significantly lowered. After executing our algorithm, parameters improved their variance by 14.34% on average. The overall accuracy, quantified by the volume of the confidence ellipsoid, improved by at least 25%. The developed method for frequency adjustments for performing the EIS can also be incorporated within a measurement setup when characterizing the Li-ion cells. This is confirmed through experimental validation on a real Li-ion cell at different temperatures and SoC. For the considered states, the parameters are successfully initialized and efficiently estimated. For the case of 25 °C and 80% SoC, frequency adjustments lead to a variance decrease of 16.4% on average and ellipsoid volume decreases by nearly 20%. At 15 °C and 20% SoC, the frequency adjustments result in a variance decrease of 28.2% on average and ellipsoid volume decrease by 55%. A similar approach can be potentially applied to other electrochemical systems which require impedance characterization and precise ECM identification.

Acknowledgements

This research is carried out in the frame of EPFL – PSA Stationary Storage Study, financed by Stellantis and of the Swiss Circular Economy Model for Automotive Lithium Batteries (CircuBAT) Flagship project, with the financial support of the Swiss Innovation Agency (Innosuisse - Flagship Initiative) (FLAGSHIP PFFS-21-20).

References

- [1] S. Zhao, S. R. Duncan, and D. A. Howey, “Observability Analysis and State Estimation of Lithium-Ion Batteries in the Presence of Sensor Biases,” *IEEE Transactions on Control Systems Technology*, vol. 25, pp. 326–333, Jan. 2017. Conference Name: IEEE Transactions on Control Systems Technology.
- [2] M. Koseoglou, E. Tsioumas, D. Papagiannis, N. Jabbour, and C. Mademlis, “A Novel On-Board Electrochemical Impedance Spectroscopy System for Real-Time Battery Impedance Estimation,” *IEEE Transactions on Power Electronics*, vol. 36, pp. 10776–10787, Sept. 2021. Conference Name: IEEE Transactions on Power Electronics.
- [3] S. M. M. Alavi, A. Mahdi, S. J. Payne, and D. A. Howey, “Identifiability of Generalized Randles Circuit Models,” *IEEE Transactions on Control Systems Technology*, vol. 25, pp. 2112–2120, Nov. 2017. Conference Name: IEEE Transactions on Control Systems Technology.
- [4] S. M. M. Alavi, C. R. Birkl, and D. A. Howey, “Time-domain fitting of battery electrochemical impedance models,” *Journal of Power Sources*, vol. 288, pp. 345–352, Aug. 2015.
- [5] P. Iurilli, C. Brivio, and V. Wood, “On the use of electrochemical impedance spectroscopy to characterize and model the aging phenomena of lithium-ion batteries: a critical review,” *Journal of Power Sources*, vol. 505, p. 229860, Sept. 2021.
- [6] J. R. Macdonald and J. A. Garber, “Analysis of Impedance and Admittance Data for Solids and Liquids,” *Journal of The Electrochemical Society*, vol. 124, p. 1022, July 1977. Publisher: IOP Publishing.
- [7] M. E. Orazem and B. Tribollet, *Electrochemical impedance spectroscopy*. Hoboken, New Jersey: John Wiley & Sons, Inc., 2017. OCLC: 1104176375.
- [8] J. Nocedal and S. J. Wright, *Numerical optimization*. Springer series in operations research, New York: Springer, 2nd ed ed., 2006. OCLC: ocm68629100.
- [9] K. Geuten, T. Massingham, P. Darius, E. Smets, and N. Goldman, “Experimental Design Criteria in Phylogenetics: Where to Add Taxa,” *Systematic biology*, vol. 56, pp. 609–22, Sept. 2007.
- [10] P. Goos and B. Jones, *Optimal design of experiments: a case study approach*. Hoboken, N.J: Wiley, 2011.
- [11] A. Pozzi, G. Ciaramella, K. Gopalakrishnan, S. Volkwein, and D. M. Raimondo, “Optimal Design of Experiment for Parameter Estimation of a Single Particle Model for Lithiumion Batteries,” in *2018 IEEE Conference on Decision and Control (CDC)*, (Miami Beach, FL), pp. 6482–6487, IEEE, Dec. 2018.
- [12] A. P. Schmidt, M. Bitzer, A. W. Imre, and L. Guzzella, “Experiment-driven electrochemical modeling and systematic parameterization for a lithium-ion battery cell,” *Journal of Power Sources*, vol. 195, pp. 5071–5080, Aug. 2010.
- [13] P. Pillai, S. Sundaresan, K. R. Pattipati, and B. Balasingam, “Optimizing Current Profiles for Efficient Online Estimation of Battery Equivalent Circuit Model Parameters Based on Cramer–Rao Lower Bound,” *Energies*, vol. 15, p. 8441, Nov. 2022.
- [14] M. J. Rothenberger, D. J. Docimo, M. Ghanaatpishe, and H. K. Fathy, “Genetic optimization and experimental validation of a test cycle that maximizes parameter identifiability for a Li-ion equivalent-circuit battery model,” *Journal of Energy Storage*, vol. 4, pp. 156–166, Dec. 2015.
- [15] X. Du, J. Meng, Y. Zhang, X. Huang, S. Wang, P. Liu, and T. Liu, “An Information Appraisal Procedure: Endows Reliable Online Parameter Identification to Lithium-Ion Battery Model,” *IEEE Transactions on Industrial Electronics*, vol. 69, pp. 5889–5899, June 2022. Conference Name: IEEE Transactions on Industrial Electronics.

- [16] J. R. Macdonald and L. D. Potter, “A flexible procedure for analyzing impedance spectroscopy results: Description and illustrations,” *Solid State Ionics*, vol. 24, pp. 61–79, June 1987.
- [17] M. Abaspour, K. R. Pattipati, B. Shahrrava, and B. Balasingam, “Robust Approach to Battery Equivalent-Circuit-Model Parameter Extraction Using Electrochemical Impedance Spectroscopy,” *Energies*, vol. 15, p. 9251, Dec. 2022.
- [18] B. Ospina Agudelo, W. Zamboni, E. Monmasson, and G. Spagnuolo, “Identification of battery circuit model from EIS data,” (Saint Pierre d’Oléron, France), hal-02915697, June 2019.
- [19] U. Tröltzsch, O. Kanoun, and H.-R. Tränkler, “Characterizing aging effects of lithium ion batteries by impedance spectroscopy,” *Electrochimica Acta*, vol. 51, pp. 1664–1672, Jan. 2006.
- [20] S. M. R. Islam, S.-Y. Park, and B. Balasingam, “Unification of Internal Resistance Estimation Methods for Li-Ion Batteries Using Hysteresis-Free Equivalent Circuit Models,” *Batteries*, vol. 6, p. 32, June 2020.
- [21] Y. Wu, S. Sundaresan, and B. Balasingam, “Battery Parameter Analysis through Electrochemical Impedance Spectroscopy at Different State of Charge Levels,” *Journal of Low Power Electronics and Applications*, vol. 13, p. 29, Apr. 2023.
- [22] S. Wang, J. Zhang, O. Gharbi, V. Vivier, M. Gao, and M. E. Orazem, “Electrochemical impedance spectroscopy,” *Nature Reviews Methods Primers*, vol. 1, p. 41, June 2021.
- [23] T. Söderström and P. Stoica, *System identification*. Prentice Hall international series in systems and control engineering, New York, NY: Prentice-Hall, reprint ed.
- [24] G. Instruments, “Accuracy Contour Plots – Measurement and Discussion.”
- [25] BioLogic, “How to read EIS accuracy contour plots.”
- [26] D. Lerro and Y. Bar-Shalom, “Tracking with debiased consistent converted measurements versus EKF,” *IEEE Transactions on Aerospace and Electronic Systems*, vol. 29, pp. 1015–1022, July 1993. Conference Name: IEEE Transactions on Aerospace and Electronic Systems.
- [27] M. Paolone, J.-Y. Le Boudec, S. Sarri, and L. Zanni, “Static and recursive PMU-based state estimation processes for transmission and distribution power grids,” in *Advances in Power System Modelling, Control and Stability Analysis* (Milano, ed.), pp. 189–239, Institution of Engineering and Technology, Sept. 2016.
- [28] S. M. Kay, *Fundamentals of statistical signal processing*. Prentice Hall signal processing series, Englewood Cliffs, N.J: Prentice-Hall PTR, 1993.
- [29] F. Nielsen, “An Elementary Introduction to Information Geometry,” *Entropy (Basel, Switzerland)*, vol. 22, Aug. 2018.
- [30] A. J. Wilson, “Volume of n-dimensional ellipsoid,” *Scientia Acta Xaveriana*, vol. 1, no. 1, pp. 101–106, 2009.